MASTER SEMESTER PROJECT

Power to H_2 - Tank to Power

Diego Vermeire

Supervised by
Pr. François Maréchal
Yi Zhao

Industrial Processes and Energy Systems Engineering (IPESE) Laboratory
Ecole Polytechnique Fédérale de Lausanne

Fall 2023

November 20, 2023

Abstract

The urgent imperative to curtail carbon emissions necessitates the extensive implementation of renewable technologies. However, the intermittent nature of renewables poses challenges to sustainable and efficient energy storage. This project focuses on exploring long-term energy storage systems, evaluating both their cost-effectiveness and efficiency.

Utilizing the well-established concept of Power to X to Power, the project employs modeling techniques to analyze various technologies, enabling a comprehensive comparison of long-term energy storage systems based on efficiency and cost.

The first candidate for energy storage is Power to Heat to Power, involving a model that calculates the cost and efficiency of a heat storage device. This model incorporates components such as a heat pump cycle and a thermal engine cycle, assessing different temperatures and technical properties. A second candidate involves storing excess electricity as hydrogen. The second model, Power to Hydrogen Tank to Power, focuses on the storage of excess electricity in the form of hydrogen. It examines the use of Solid Oxide Electrolyzer Cells (SOEC) and Solid Oxide Fuel Cells (SOFC) in both liquid and gaseous hydrogen storage systems, assessing their potential as effective energy storage technologies.

The ultimate objective is to facilitate a comparative analysis of different Power to X to Power technologies in terms of efficiency and investment cost. This research contributes to understanding viable long-term energy storage solutions, informing strategic decisions for a sustainable and low-carbon future.

Acknowledgements

This semester project is an integral part of my Master's program in Energy Science and Technology at EPFL (Ecole Polytechnique Fédérale de Lausanne). I am profoundly grateful for the exceptional assistance and invaluable guidance provided by Yi Zhao and Jingjing Liang. Their unwavering support and expert supervision were indispensable in ensuring the successful execution of this project. Moreover, I extend special thanks to Professor Maréchal for his constructive feedback on the project and for granting me the opportunity to undertake this research at the IPESE at EPFL. A big thanks is also due to the entire team at the IPESE-lab for their warm welcome, support, and collaboration. Their expertise, cooperation, and welcoming atmosphere significantly contributed to the success and enriching experience of this project. I am sincerely grateful for their assistance and cooperation throughout the research process.

Table of Contents

List of Figures

List of Tables

1 Project Overview and Goals

1.1 Current National Context

In alignment with the Paris Agreement, Switzerland updated its Nationally Determined Contribution (NDC) in 2020, committing to achieve net zero emissions by 2050 and a 50 % reduction in greenhouse gas (GHG) emissions by 2030 compared to 1990 levels. As of 2022, Switzerland has achieved a notable 19.88% reduction in GHG emissions, emitting 35.38 million tons of equivalent [1]. However, offsetting the remaining 30% within the next eight years poses a significant challenge. Switzerland's long-term climate strategy outlines ten strategic principles guiding national climate policy, encompassing emissions reduction targets for various sectors such as buildings, industry, transport, agriculture, and others[2].

The country's energy consumption is largely dominated by petroleum and motor fuels (43%), followed by electricity (26%), and gas (15%) [3]. To address the imperative reduction in greenhouse gas emissions, there is a growing emphasis on substituting fossil-fueled energy with renewable electricity production. This transition is expected to substantially increase electricity demand from 62 TWh to 80-90 TWh by 2050, constituting a 25-40% rise from current consumption[4].

Renewable electricity sources, particularly wind and solar, hold significant potential in providing cleaner energy solutions, given their decreasing costs and increasing efficiency [5]. However, their intermittent nature necessitates innovative and cost-effective electricity storage solutions for both short and long-term needs.

1.2 Power to X to Power

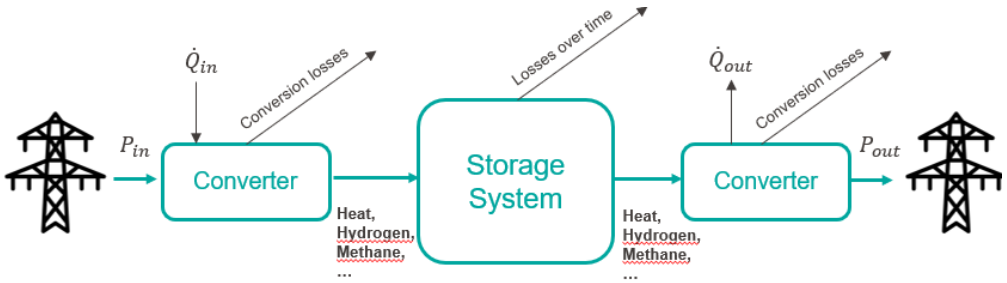

Figure 1: Overview of a typical Power to X to Power electricity storage system

As mentioned, the intermittent nature of renewable energy sources necessitates innovative solutions for efficient and cost-effective electricity storage on both short and long-term scales. Power-to-X-to-Power, a pivotal concept in this endeavor, involves the conversion of surplus electricity P_{in} into diverse storage mediums denoted as "X", which can subsequently be reconverted back into electricity P_{out} when demand arises. The versatile "X" encompasses various possibilities, such as heat (transferred through heat pumps and thermal engines [6]), hydrogen (generated via electrolysis and utilized in a fuel cell [7]), methane (produced, for example, from hydrogen and carbon dioxide [8]), or even methanol (manufactured using hydrogen and carbon dioxide[9]).

Through modeling of different Power-to-X-to-Power technologies, the overarching goal of this project is to estimate and compare the efficiency and capital expenditure costs associated with various long-term energy storage applications. It is essential to note that factors beyond efficiency

and capital expenditure costs, including convenience and network compatibility, profoundly influence the suitability of a specific technology. For instance, despite being more expensive and less efficient, producing methane from hydrogen is often favored due to its ease of integration into existing city gas networks [10].

1.2.1 Power to Heat to Power

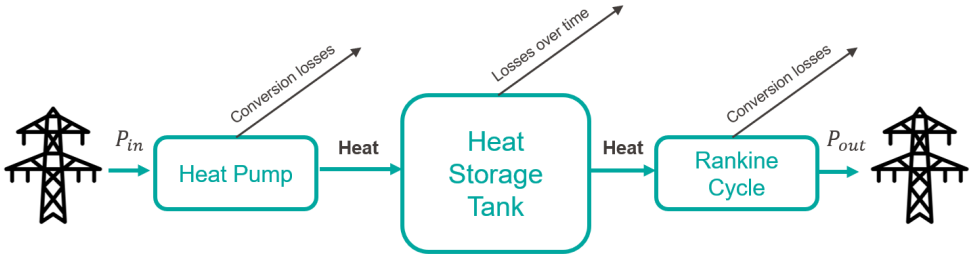

Figure 2: Overview of a typical Power to Heat to Power electricity storage system [6]

In a previous report written by Romain Phan [6], a power-to-heat-to-power model was developed. Romain Phan's model for Power-to-Heat-to-Power focused on the design and analysis of a heat storage system for electricity storage over medium-term durations, ranging from 1 to 6 months. The model incorporates various parameters, such as external and storage temperatures, insulation thickness, storage capacity, charging time, and others, to simulate the cost, efficiency, and profitability of the proposed system. The system comprises a heat pump cycle for heat generation, a heat storage tank for heat storage, and a thermal engine cycle for electricity generation from heat, utilizing a Rankine cycle.

The heat storage system shows promise for short- to medium-term storage (1 to 6 months), despite its modest efficiency around 30%, influenced by heat losses, compressor and turbine efficiency in the heat pump and Rankine cycle, and exergy losses in temperature differences at the heat exchangers. Key drivers of system performance are storage time and capacity. Storage time dictates insulating material thickness, crucial for efficiency. Simultaneously, accurate determination of storage capacity is vital for optimal efficiency.

In conclusion, achieving profitability in around 10 years seems feasible, possibly less with parameter adjustments. This underscores the critical role of carefully considering storage time and capacity for successful Power-to-Heat-to-Power system implementation.

2 Literature Review

Extensive research has been directed towards developing models for electrolyzers, particularly PEM and SOEC types, highlighted in studies by Falcão [11], Leonide [12], and Klotz [13]. These works also delve into corresponding fuel cell technologies. Moreover, the modeling of SOEC and SOFC cells has been richly explored in literature, with significant contributions from authors like Menon [14], Ba [15], Meier [16], and Bianchi [17], among others [18, 19, 20, 21]. This comprehensive review of existing studies was crucial in shaping the modeling approach for this project, especially in bridging initial knowledge gaps.

3 Power to H_2-tank to Power

3.1 Overview

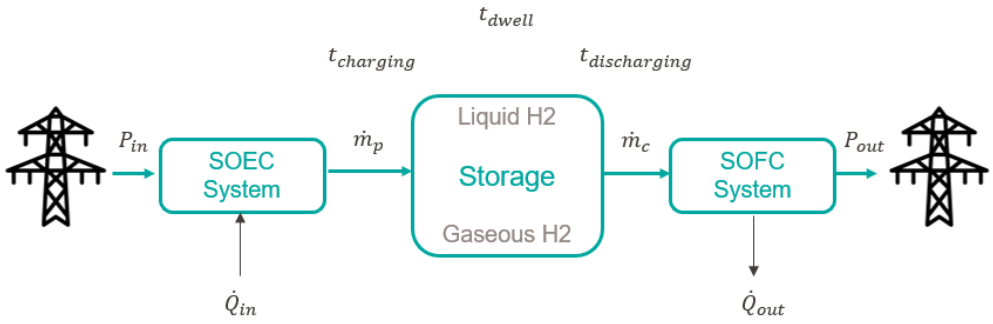

Figure 3: Overview of the developed Power to Hydrogen Tank to Power model

Power-to-Hydrogen tank-to-Power (PtH2tP) represents an innovative electricity storage concept. This transformative approach involves the conversion of surplus electricity P_{in} into hydrogen $\dot{m}_p$ through water electrolysis, storing produced hydrogen, and later using stored hydrogen $\dot{m}_c$ in a fuel cell to generate electricity when needed. PtH2tP is a key player in addressing the intermittency of renewable energy sources, providing versatile and efficient means of storing excess electricity in the long-term.

Table 1: Variables in the Power-to-Hydrogen Tank-to-Power Model Overview

Variable	**Meaning**	**Unit**
P_{in}	Excess power from the grid	[W]
$\dot{m}_p$	Hydrogen production rate	[W]
$\dot{m}_c$	Hydrogen consumption rate	[W]
P_{out}	Output power injected into the grid	[W]
$\dot{Q}_{in}$	Heat input rate of the SOEC system	[W]
$t_{charging}$	Duration of charging storage tank/duration of SOEC operation	[days]
t_{dwell}	Dwell duration of H2 inside the storage tank	[days]
$t_{discharging}$	Discharging duration of tank/duration of SOFC operation	[W]
$\dot{Q}_{out}$	Heat output rate from SOFC operation	[W]

In the modeling of a Power-to-Hydrogen Tank-to-Power system, it is imperative to account for two essential forms of energy: electricity and heat. The operation of a Solid Oxide Electrolysis Cell (SOEC) necessitates electrical power, while a Solid Oxide Fuel Cell (SOFC) generates electrical power for consumption. Moreover, the storage of hydrogen involves the use of electricity for processes like H_2 compression or liquefaction. Simultaneously, heat plays a crucial role in the system, given the high operating temperatures of SOEC and SOFC. The reactants and products of these cells are at elevated temperatures, influencing the overall system dynamics. Furthermore, the electrolysis reaction in a SOEC necessitates heat, particularly when not operated under the thermoneutral potential [1].

[1]The thermoneutral potential of a SOEC refers to the condition where the overall reaction neither absorbs nor releases heat[22].

Conversely, a Solid Oxide Fuel Cell (SOFC) generates heat during its operation, contributing to the energy dynamics of the system.

The above emphasizes the significance of a comprehensive heat and electrical model. The decision has been made to initially focus on modeling the electrical aspect. Although the heat model was initiated, it was omitted from the current report due to inaccuracies that need refinement in subsequent stages of research.

3.1.1 Technology

Hydrogen energy storage, involving electrolysis where electricity splits water into hydrogen and oxygen, employs various technologies like alkaline, proton exchange membrane (PEM), and solid oxide electrolysis for effective electrical to hydrogen energy conversion [23]. Additionally, the process of electrochemical oxidation in Solid Oxide Fuel Cells (SOFC) plays a pivotal role in this system. This stored hydrogen is then reconverted into electricity using fuel cells.

3.1.2 Required Equipment

Various equipments are essential for storing hydrogen as an energy source. This includes hydrogen storage tanks, electrolyzers that split water molecules, compressors to modify hydrogen pressure or liquefiers to liquefy hydrogen and fuel cells for converting hydrogen back into electrical energy. The choice of equipment depends on factors like scale, application, hydrogen storage technique, and specific energy needs

3.1.2.1 Electrolyzer Technologies [23] [24] In this model, the choice of Solid Oxide Electrolysis Cells (SOEC) and Solid Oxide Fuel Cells (SOFC) as preferred options over alternatives like Proton Exchange Membrane (PEM) electrolysis, Alkaline Electrolysis (AE) and Alkaline Exchange Membrane, is underpinned by several critical considerations.

One pivotal factor is their high efficiency at high operating temperatures. SOEC and SOFC excel in operation at elevated temperatures, leading to superior overall efficiency in the energy conversion process. Notably, the cell efficiency of SOEC stands out, reaching up to 95% [25].

Another significant advantage lies in the syngas production capability inherent to SOEC technology. Unlike some alternatives, SOEC allows for the direct synthesis of syngas—a mixture of hydrogen and carbon monoxide—from CO2 and water. This distinctive feature enhances the system's versatility, enabling the concurrent production of syngas and hydrogen. Such flexibility opens avenues for diverse applications, including chemical synthesis processes and CO2 capture and utilisation in the steel industry [26].

Economic considerations further contribute to the preference for SOEC and SOFC. While acknowledging that these systems may entail higher upfront costs, ongoing research and development initiatives point to the potential for cost reduction. The accrued expertise from existing SOEC plants is instrumental in driving down material costs, rendering them economically competitive. Moreover, when compared to alternative technologies, SOEC systems demonstrate lower material costs, bolstering their viability and attractiveness in the context of the power-to-H_2-tank-to-Power model [27].

In summary, the selection of SOEC and SOFC for the model is driven by their high efficiency, syngas production capability, ongoing cost reduction potential and overall suitability for integration into the envisioned Power-to-Hydrogen Tank-to-Power system.

3.1.3 Advantages and Drawbacks of H_2-storage [28]

Advantages of Hydrogen Storage

- **High Energy Density**: Hydrogen offers a high energy density by weight, allowing for efficient energy storage in a compact and lightweight form.
- **Long-term Storage:** Hydrogen can be stored indefinitely without significant energy loss, making it suitable for long-term storage and seasonal energy balancing.
- **Scalability:** Hydrogen energy storage systems can be scaled up or down to meet diverse applications, from small residential setups to large-scale grid storage.
- **Harmless by-products:** The conversion of hydrogen back into electricity produces only water as a by-product, offering a "clean and environmentally friendly" energy storage solution.

Drawbacks of Hydrogen Storage

- **Energy Density by Volume:** Despite its high energy density by weight, hydrogen's energy density by volume is relatively low, necessitating large storage tanks or high-pressure systems for compact storage.
- **Low Efficiency:** The round-trip efficiency of hydrogen energy storage is typically 40% to 50%, lower than some other energy storage technologies like batteries.
- **High Capital Costs:** The necessary equipment, such as electrolysers, liquefiers or compressors, and fuel cells, can be expensive, resulting in higher initial capital costs compared to alternative energy storage solutions.
- **Infrastructure Challenges:** The lack of an established hydrogen infrastructure, including pipelines and refuelling stations, poses a barrier to widespread adoption.
- **Safety Concerns:** Hydrogen is highly flammable, requiring stringent safety measures in its storage and transportation to prevent accidents.

3.2 Electrical Model

The following section outlines the electrical model without accounting for any heat considerations. As depicted in Figure 3, the developed model predominantly consists of three systems: Solid Oxide Electrolyser System, Solid Oxide Fuel Cell System, and a Storage System. To provide a thorough understanding of the model, the model will be discussed in terms of these three systems.

3.2.1 Approach

As discussed in Section 2, the adopted approach is deemed innovative. Unlike many existing models, the innovation lies in commencing the model from the J-V characteristics of SOEC and SOFC. This unique approach involves starting at a foundational level and progressing upward—first to a stack level, then to a system level, and ultimately integrating with the grid to account for electricity price fluctuations. This methodology aligns with a techno-economic standpoint, conducting both cost and technical analyses with a focus on efficiency as a key metric.

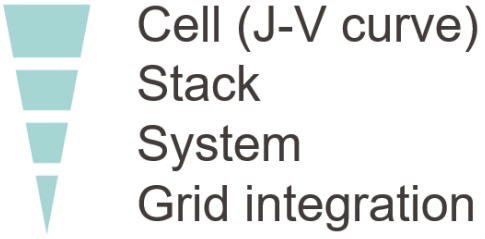

Figure 4: Bottom-up approach of the developed Power to H_2-Tank to Power model

3.2.2 Solid Oxide Electrolyser System

As shown in Figure 5 to construct the system model, the initial step involves modeling the SOEC cell. Progressing upwards, the modeling extends to a SOEC stack. Finally, by integrating multiple SOEC stacks and incorporating Balance of Plant (BOP) considerations, a comprehensive SOEC systems model is derived. The primary outputs of this model encompass the SOEC capital expenditure (Capex) cost and its electrical efficiency.

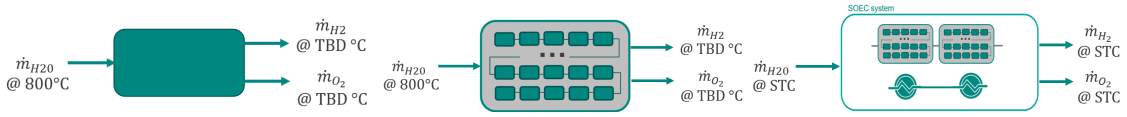

(a) SOEC cell (b) SOEC Stack (c) SOEC System

Figure 5: Overview of Various Structural Configurations in SOEC Model

3.2.2.1 SOEC Cell

The electrical cell model of the Solid Oxide Electrolysis Cell (SOEC), as illustrated in Figure 5a [2], operates as a black box. Water enters the cell at a specified temperature, referred to as T_{cell}, with a current default setting of 800°C. Within the cell, electrolysis of water occurs, leading to the generation of H_2 and O_2, which exit the cell at a temperature determined by the operational state of the cell. To provide a comprehensive understanding of the model's parameters, Table 2 enumerates all model's input parameters initially set to default values, which can be modified if needed. The significance of these parameters will become clearer as we delve into the discussion of the J-V characteristic of the cell.

[2]The above figures represent the electrochemical reaction while focusing on flow transport. At this stage, certain parameters like input heat ($\dot{Q}_{in}$) and input power (P_{in}) are intentionally excluded from the representation.

Input Parameters	Meaning	Default Value	Units
J	Cell Current Density	0.5	$[\frac{A}{cm^2}]$
T	Cell Operating Temperature	800	[°C]
p_{H_2}	Hydrogen Cell Partial Pressure	0.1	[ ]
p_{H20}	Water Cell Partial Pressure	0.9	[ ]
p_{O_2}	Oxygen(Air) Cell Partial Pressure	0.21	[ ]
Output Parameters	**Meaning**	**Default Value**	**Units**
E_{cell}	Cell Operating Voltage	TBD	[V]

Table 2: Overview of SOEC cell electrical model input and output parameters

Chemical reaction : In a Solid Oxide Electrolysis Cell (SOEC), fundamental chemical reactions occur at the anode and cathode interfaces, driving the electrolysis process for water splitting. At the anode-electrolyte interface, oxygen ions (O^{2-}) undergo oxidation according to Equation 1:

$$\text{Anode: } O^{2-} \rightarrow \frac{1}{2}O_2 + 2e^- \tag{1}$$

Simultaneously, at the cathode-electrolyte interface, water is reduced according to Equation 2:

$$\text{Cathode: } H_2O + 2e^- \rightarrow H_2 + O^{2-} \tag{2}$$

The net reaction for one mole of water involves the reduction of water at the cathode and the oxidation of oxygen ions at the anode. As can be seen on Figure 6, the net reaction entails:

$$\text{Net Reaction: } H_2O \rightarrow H_2 + \frac{1}{2}O_2 \tag{3}$$

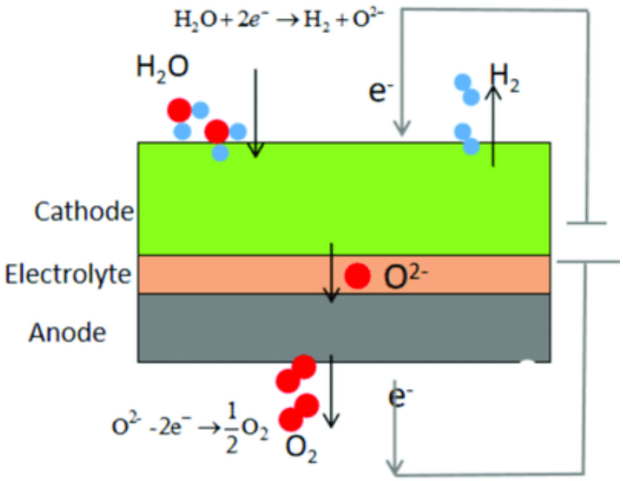

Figure 6: Schematic of solid oxide electrolysis cell (SOEC) working principle [29]

These electrochemical processes take place within the SOEC, operating at elevated temperatures between 500 and 1000 °C. The cell utilizes a solid oxide electrolyte, typically composed of ZrO2 doped with Y2O3 (YSZ) [30] [**fergus_electrolytes_2006**], to enable the ionic conduction necessary for the electrolysis reactions. The fuel electrode (cathode) and oxygen electrode (anode) materials play crucial roles in facilitating the reduction and oxidation reactions, respectively, and are often composed of materials such as Ni-doped YSZ and LSM. The effective operation of the SOEC relies on the intricate balance of material properties and operating conditions to achieve efficient hydrogen and oxygen gas production through high-temperature electrolysis.

J-V Charcateristics of SOEC : In the methodology for computing the J-V characteristics of the Solid Oxide Electrolysis Cell (SOEC), a series of equations are employed to determine the operating cell potential (E_{cell}) [22] given a certain cell current density (J_{cell}). Firstly, the reversible cell potential (E^0) is calculated using the Gibbs free energy change (ΔG), the Faraday constant (F), and the temperature (T):

$$E^0 = -Z \cdot F \cdot \frac{\Delta G}{T} \tag{4}$$

in units of volts [V].

Subsequently, the Nernst equation is applied to incorporate the effect of partial pressures of hydrogen (p_{H2}), oxygen (p_{O2}), and water vapor (p_{H2O}) on the reversible cell potential under the given operating conditions:

$$E^0_{\text{cell}} = E^0 - \frac{RT}{ZF} \cdot \ln\left(\frac{p_{\text{H2O}}}{p_{\text{H2}} \cdot \sqrt{p_{\text{O2}}}}\right) \tag{5}$$

in units of volts [V].

The activation overpotential (η_a) is computed using the Butler-Volmer equation, combining contributions from anodic and cathodic reactions:

$$\eta_a = \eta_{(a,\text{anode})} + \eta_{(a,\text{cathode})} \tag{6}$$

The concentration overpotential (η_{conc}) is considered negligible for the non-fuel electrode. More complex equations have been used for the computation of the concentration overpotential (η_{conc}), according to (equations 10&11 [31]).

The ohmic overpotential (η_{ohm}) is determined by multiplying the cell current density (J_{cell}) with the ohmic resistance (R_{ohm}):

$$\eta_{\text{ohm}} = J_{cell} \cdot R_{\text{ohm}} \tag{7}$$

It is important to emphasize that the overpotential values have been computed using cell characteristics from a specific paper [31], wherein a SOEC model was developed to align with experimental

data obtained from a real SOEC cell. The values employed for calculating the overpotentials are therefore specific to this particular model, corresponding to a distinct type of SOEC cell tested in a laboratory setting. While the methodology and formulas are consistent across all possible SOEC cells, it is important to acknowledge the specificity of the obtained values. Nonetheless, future contributors can seamlessly adapt these calculations to suit the characteristics of their own studied cells, underscoring the versatility and applicability of the presented methodology.

The final step involves combining these overpotentials with the reversible cell potential to obtain the operating cell potential (E_{cell}):

$$E_{\text{cell}} = E^0_{\text{cell}} + \eta_a + \eta_{\text{conc}} + \eta_{\text{ohm}} \tag{8}$$

In conlusion this approach, incorporating these equations, provides insights into the voltage behavior of the SOEC under a fixed cell current density J_{cell}. The above equations should clarify the input parameters of the SOEC cell model mentioned in Table 2.

J-V Characteristics Curve Simulations : Figure 7 illustrates the output of the SOEC model, depicting the variation in cell operating voltages (E_{cell}) for cell current densities (J_{cell}) ranging from 0 to 2.1 A/cm^2. A distinct limiting current density (j_{lim}) becomes apparent in the figure 7. This limitation arises from constraints related to mass transport phenomena. Specifically, at higher current densities, the SOEC cell experiences an elevated rate of water consumption (H_2O), resulting in limitations imposed by mass transport phenomena associated with water.

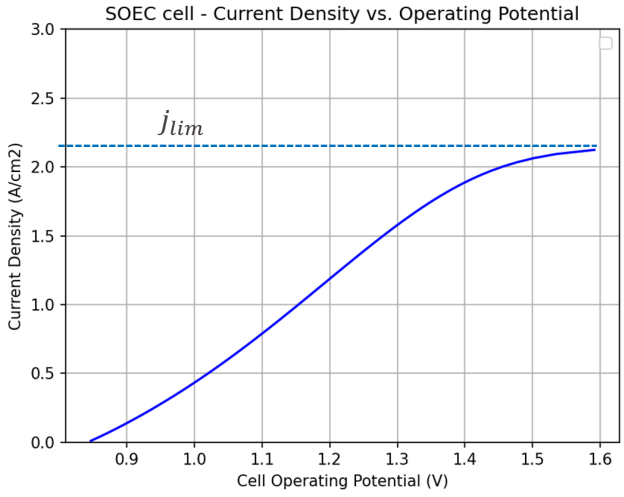

(a) SOEC cell J-V curve

Input Parameter	Numerical Value	Unit
p_{H_2}	0.1	[ ]
p_{H_2O}	0.9	[ ]
p_{O_2}	0.21	[ ]
T_{cell}	800	[°C]

(b) SOEC model Input Parameters Values

Figure 7: SOEC cell J-V Characteristic Curves

V-J Characteristics Curve Simulations : Figure 8 presents the reversible V-J curves for the studied SOEC cell, operated in SOEC mode (depicted in blue), and a cell operated in SOFC mode (depicted in green). It's noteworthy that the axes have been transposed in comparison to Figure 7. This section delves into an analysis of the injected power in a SOEC cell operating at a cell current density of 0.2 A/cm^2 and a cell operating voltage E_{cell} of 1.1 V. Figure 8a illustrates the consumed

power density $P_{\text{dens, cons}}$ by the cell.

$$P_{\text{dens, cons}} = J_{cell} \cdot E_{\text{cell}} \tag{9}$$

in units of $\frac{W}{cm^2}$.

In Figure 8b, the blue rectangle represents the useful power density $P_{\text{dens, use}}$:

$$P_{\text{dens, use}} = J_{cell} \cdot E^0_{\text{cell}} \tag{10}$$

in units of $\frac{W}{cm^2}$.

The yellow rectangle in Figure 8b represents the power density losses (heat) $P_{\text{dens, loss}}$:

$$P_{\text{dens, loss}} = P_{\text{dens, cons}} - P_{\text{dens, use}} \tag{11}$$

in units of $\frac{W}{cm^2}$.

These equations encapsulate the power dynamics within the SOEC cell, offering insights into the consumed power, useful power transformation, and losses in the form of heat.

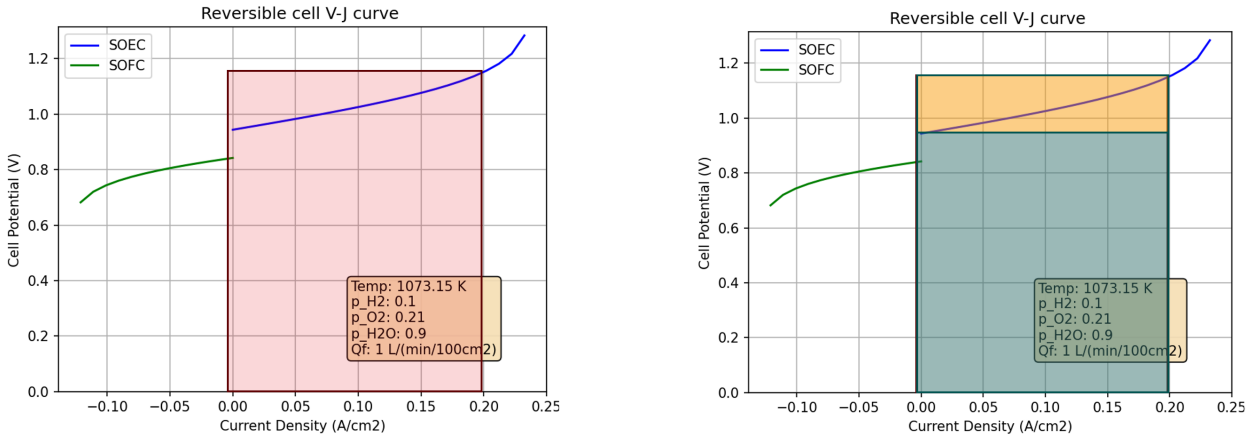

(a) Power Density Consumed

(b) Useful Power Density

Figure 8: SOEC Cell Reversible V-J Curves

3.2.2.2 SOEC Stack The electrical model of the Solid Oxide Electrolysis Stack (SOEC), illustrated in Figure 5b, functions as a black box. Water enters the stack at a designated temperature, denoted as T_{cell} and initially set at 800°C. The stack comprises multiple interconnected SOEC cells arranged in series, where the injected power and water are distributed across the cells constituting the stack. Notably, a stack is composed of 130 SOEC cells linked in series. Electrolysis of water takes place independently in each of these 130 SOEC cells, resulting in the production of H_2 and O_2. The exit temperature of these gases is contingent upon the operational status of the individual cells. The decision to employ a stack with 130 cells is based on insights derived from a prior scientific report [32], which extensively examined the cost and manufacturing aspects of a stack with the same cell count. It is important to note that all cells within a stack are considered to be operated at the same point on the J-V curve. Table 3 provides a summary of the key characteristics of the selected stack.

SOEC Parameter	Value	Units
Single Cell Rated Power	349.83	[W]
$\frac{Cells}{1Stack}$	130	[ ]
Stack Rated Power	45	[kW]
Cell Active Area	299	[cm]

Table 3: Stack Characteristics [32]

3.2.2.3 SOEC System The SOEC system model, depicted in Figure 5c, operates as a sealed system. Water enters under standard testing conditions, specifically at 25°C and atmospheric pressure. The hydrogen and oxygen exiting the SOEC cell system are assumed to leave under standard testing conditions. Within this sealed system, SOEC stacks are arranged in series along with the Balance of Plant (BOP). The BOP encompasses various components, including the heat model. As detailed in section 3.2.1, it's worth noting that the heat model requires further refinement, and therefore, it is currently not taken into consideration in the BOP. However, it is crucial to bear in mind that the SOEC system incorporates the BOP when calculating the system's capital expenditure (CAPEX) costs in further sections.

System's Size Calculations : Unlike the SOEC stack, whose number of cells or size is predetermined, the number of SOEC stacks in series within the SOEC system is variable. The specific quantity of SOEC stacks in series depends on both the cell current density at which all cells in all stacks operate and the power input P_{in} for which the SOEC system is designed. To determine the number of SOEC stacks in series within the SOEC system n_{stack} for a fixed cell current density J_{cell} and power input P_{in}, the stack power P_{stack} is first calculated. The stack power represents the power consumed by each stack under the specified conditions outlined in figure 7b and J_{cell}. The operating cell voltage E_{cell} is computed specifically for the given J_{cell} using the equations and model explained in section 3.2.2.1 (equation 3.2.2.1).

$$P_{\text{stack}} = J_{\text{cell}} \cdot E_{\text{cell}} \cdot \frac{n_{cell}}{1 \text{ stack}} \cdot A_{\text{cell}} \tag{12}$$

in units of watts $[W]$, where $\frac{n_{cell}}{1 \text{ stack}}$ is the number of cells in each stack and A_{cell} is the SOEC's cell active area.

Finally, the number of stacks within the SOEC system is computed using the equation:

$$n_{\text{stack}} = \frac{P_{\text{in}}}{P_{\text{stack}}} \tag{13}$$

These calculations enable the determination of the required number of SOEC stacks in series for a given system design (P_{in} and J_{cell}).

System's Electrical Efficiency Calculations : The determination of the SOEC system's electrical efficiency involves parameters analyzed in distinct steps. Firstly, the power consumed by the entire system P_{cons} is computed, using the cell current density J_{cell}, cell operating voltage E_{cell}, the number of cells in each stack $\frac{n_{cell}}{1 \text{ stack}}$, the cell active area A_{cell} and the number of stacks in the

SOEC system n_{stacks} (see equation 13). This is expressed as

$$P_{\text{cons}} = J_{\text{cell}} \cdot E_{\text{cell}} \cdot \frac{n_{\text{cells}}}{1 \text{ stack}} \cdot n_{\text{stacks}} \cdot A_{cell} \tag{14}$$

in units of watts (W).

Subsequently, the total system's hydrogen production rate $\dot{m}_{\text{H}_2}$ is calculated, using the total number of cells in the system n_{tot}, the molar mass of hydrogen M_{H_2}, the active cell area A_{cell}, the Faraday constant F and cell current density J_{cell}

$$n_{\text{tot}} = \frac{n_{\text{cells}}}{1 \text{ stack}} \cdot n_{\text{stacks}} \tag{15}$$

$$\dot{m}_{\text{H}_2} = M_{\text{H}_2} \cdot \frac{J_{\text{cell}}}{2 \cdot F} \cdot n_{\text{total}} \cdot A_{\text{cell}} \tag{16}$$

in units of kilograms per second $[\frac{kg}{s}]$. In literature, hydrogen production rates are commonly expressed in $[W]$ using the higher heating value of hydrogen HHV_{H_2} to transition from $[\frac{kg}{s}]$ towards $[W]$.

Finally, the electrical efficiency of the entire system (η_{ele}) is computed using the equation

$$\eta_{\text{ele}} = \frac{\dot{m}_{\text{H}_2} \cdot HHV_{\text{H}_2}}{P_{\text{cons}}} \tag{17}$$

considering the higher heating value of hydrogen (HHV_{H_2}). This efficiency metric is dimensionless, quantifying the electrical efficiency while excluding the influence of input heat into the system, as mentioned in section 3.2.1.

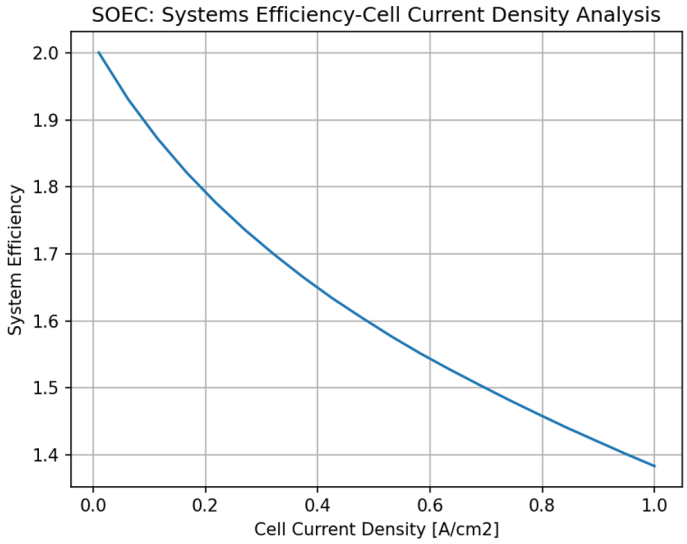

Figure 9: SOEC system's electrical efficiency versus cell current density

Figure 9 demonstrates the relationship between the electrical efficiency of the SOEC system and varying cell current densities J_{cell}. It shows a declining trend in electrical efficiency as the cell current density increases. A noteworthy aspect is the y-axis scale for electrical efficiency, extending beyond 1. This anomaly arises because the analysis currently only considers electrical efficiency, neglecting the input heat. As SOEC systems require heat alongside electrical input, not accounting for this thermal energy in the efficiency denominator skews the results, leading to an electrical efficiency greater than 1.

System's Cost Calculations : The cost of the SOEC system is primarily determined by two factors: the cost of the SOEC stacks and the Balance of Plant (BOP) cost. While further refinement is still needed for the heat model, it is however already possible to incorporate the Balance of Plant (BOP) costs in the current analysis. Utilizing information from a previous IPESE lab paper [32] and the Lawrence Berkeley National Laboratory [33] [34], an estimated cost of $800[\frac{\$}{kW}]$ is considered for SOEC/SOFC cells. The SOEC system's capital expenditure (capex) cost is computed by first determining the rated system power $P_{\text{rated, system}}$ using the equation:

$$P_{\text{rated, system}} = 349.83[W] \cdot n_{\text{stacks}} \tag{18}$$

in units of watts [W], where n_{stacks} is the number of stacks in the SOEC system (see equation 13). The value of $349.83[W]$ represents the rated power of one stack, as per Table 3.

Subsequently, the SOEC system's capex cost $Capex_{\text{system, SOEC}}$ is determined by the equation:

$$Capex_{\text{system, SOEC}} = 800[\frac{\$}{kW}] \cdot \frac{P_{\text{rated, system}}}{1000} \tag{19}$$

in units of dollars [$].

Based on internal discussions and literature review, it has been decided to consider the cost of the BOP equal to the SOEC system's capex cost $Capex_{\text{system, SOEC}}$.

Finally, accounting for both BOP and SOEC costs, the total SOEC system's capex cost $Capex_{\text{tot, SOEC}}$ is computed as:

$$Capex_{\text{tot, SOEC}} = 2 \cdot Capex_{\text{system, SOEC}} \tag{20}$$

in units of dollars [$].

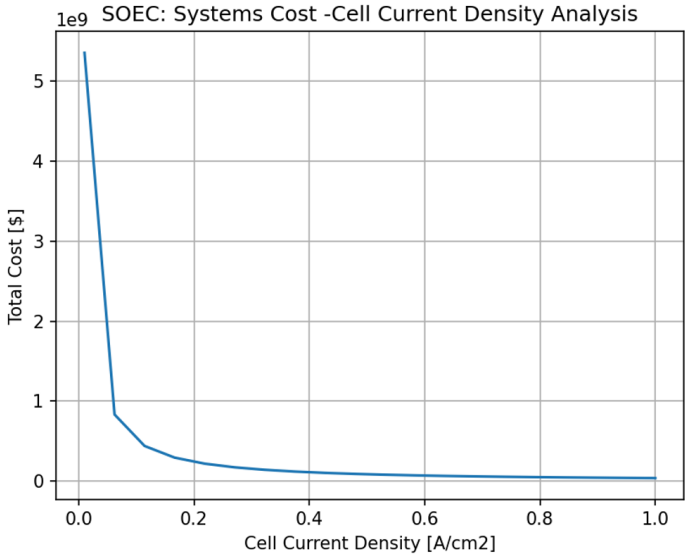

Figure 10: Total SOEC system's cost versus cell current density

Figure 10 illustrates the total capex cost of the SOEC system across different cell current densities J_{cell}. The trend indicates a decrease in total cost with an increase in cell current density as the number of stacks in the SOEC system n_{stacks} decreases.

Cost Efficiency Dilemma : Figure 11 presents the relationship between the electrical efficiency of the SOEC system and its total capex cost. A dilemma becomes evident, as operating at higher electrical efficiency results in a higher total capex cost for the SOEC system, while lower electrical efficiencies correspond to lower total costs. It is important to note that each point along the curve in Figure 11 corresponds to a specific cell current density J_{cell}.

In conclusion, a dilemma arises between the electrical efficiency of the SOEC system and its total system cost. Additionally, it has been demonstrated that the cell current density at which the SOEC cells operate significantly influences the total cost of the system and its electrical efficiency.

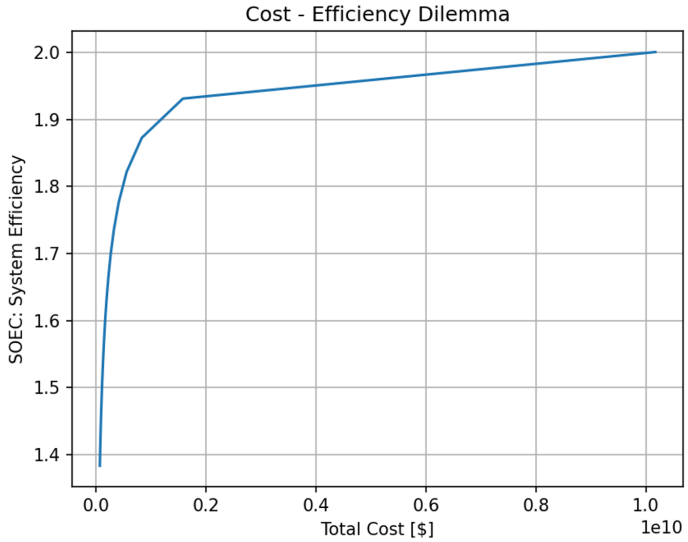

Figure 11: SOEC system's efficiency versus total SOEC system's cost

3.2.3 Solid Oxide Fuel Cell System

To construct the Solid Oxide Fuel Cell system model (SOFC), the initial step involves modeling the SOFC cell. Progressing upwards, the modeling extends to a SOFC stack. Finally, by integrating multiple SOFC stacks and incorporating Balance of Plant (BOP) considerations, the comprehensive SOFC systems model is derived. The primary outputs of this model encompass the SOFC capital expenditure (Capex) cost and its electrical efficiency.

3.2.3.1 SOFC cell

The electrical cell model of the Solid Oxide Fuel Cell (SOFC), operates as a black box. hydrogen and oxygen enter the cell at a specified temperature, referred to as T_{cell}, with a current default setting of 800°C. Within the cell, electrochemical oxidation of hydrogen occurs, leading to the generation of H_2O , which exits the cell at a temperature determined by the operational state of the cell, and electricity. To provide a comprehensive understanding of the model's parameters, Table 2 enumerates all model's input parameters initially set to the values as depicted in Figure 12b, which can be modified if needed. The significance of these parameters will become clearer as we delve into the discussion of the J-V characteristic of the cell.

Chemical Reaction: In a Solid Oxide Fuel Cell (SOFC), the core chemical reactions occur at the anode and cathode, facilitating the electrochemical conversion of fuel to electricity. At the anode-electrolyte interface, hydrogen undergoes oxidation as per the following equation:

$$\text{Anode: } H_2 + O^{2-} \rightarrow H_2O + 2e^- \tag{21}$$

Concurrently, at the cathode-electrolyte interface, oxygen is reduced in this reaction:

$$\text{Cathode: } \frac{1}{2}O_2 + 2e^- \rightarrow O^{2-} \tag{22}$$

The net reaction for the SOFC involves the oxidation of hydrogen at the anode and the reduction of oxygen at the cathode, as depicted in a corresponding figure. This process occurs at high temperatures, typically between 500 and 1000°C, using a solid oxide electrolyte such as for example YSZ. The electrodes, usually consisting of materials like Ni-YSZ for the anode and LSM for the cathode, are crucial for efficient reaction kinetics [35]. The SOFC's effectiveness hinges on the careful selection of materials and operational conditions to optimize electricity generation through these electrochemical reactions.

J-V Characteristics of SOFC: In the methodology for determining the J-V characteristics of the Solid Oxide Fuel Cell (SOFC), equations are utilized to calculate the cell's operating potential (E_{cell}) [22] for a given cell current density (J_{cell}). The reversible cell potential (E^0) in SOFCs is calculated considering the Gibbs free energy change (ΔG), the Faraday constant (F), and temperature (T) in the same way as for the SOEC cell (see equation 3.2.2.1).

Subsequently, the Nernst equation adjusts E^0 for SOFCs, considering partial pressures of hydrogen, oxygen and water, using the same formula as as for the SOEC cell (see equation 3.2.2.1). At this stage, the key distinction between SOEC and SOFC lies in the differing values of model parameters, notably the partial pressures of oxygen p_{O_2}, hydrogen p_{H_2}, and water p_{H_2O}.

The activation overpotential (η_a) is computed using the Butler-Volmer equation, combining contributions from anodic and cathodic reactions:

$$\eta_a = \eta_{(a,\text{anode})} + \eta_{(a,\text{cathode})} \tag{23}$$

The concentration overpotential (η_{conc}) is considered negligible for the non-fuel electrode. More complex equations have been used for the computation of the concentration overpotential (η_{conc}), according to (equations 10&11 [31]).

The ohmic overpotential (η_{ohm}) is determined by multiplying the cell current density (J_{cell}) with the ohmic resistance (R_{ohm}):

$$\eta_{\text{ohm}} = J_{cell} \cdot R_{\text{ohm}} \tag{24}$$

In the same way, as for the SOFC cell, it is important to emphasize that the overpotential values have been computed using cell characteristics from a specific paper [31], wherein a SOFC model was

developed to align with experimental data obtained from a real SOFC cell. The values employed for calculating the overpotentials are therefore specific to this particular model, corresponding to a distinct type of SOFC cell tested in a laboratory setting. While the methodology and formulas are consistent across all possible SOFC's.

The final step involves combining these overpotentials with the reversible cell potential to obtain the operating cell potential (E_{cell}):

$$E_{\text{cell}} = E^0_{\text{cell}} - \eta_a - \eta_{\text{conc}} - \eta_{\text{ohm}} \tag{25}$$

This approach elucidates the voltage behavior of SOFCs under varying current densities, aligning with the parameters in Figure 12b.

J-V Characteristics Curve Simulations : Figure 12 illustrates the output of the SOFC model, depicting the variation in cell operating voltages (E_{cell}) for cell current densities (J_{cell}) ranging from -1.2 to 0 A/cm^2. A distinct limiting current density (j_{lim}) becomes apparent in Figure 12. This limitation arises from constraints related to mass transport phenomena. Specifically, at more negative current densities, the SOFC cell experiences an elevated rate of hydrogen and oxygen consumption (H_2 and O_2), resulting in limitations imposed by mass transport phenomena associated with hydrogen and oxygen.

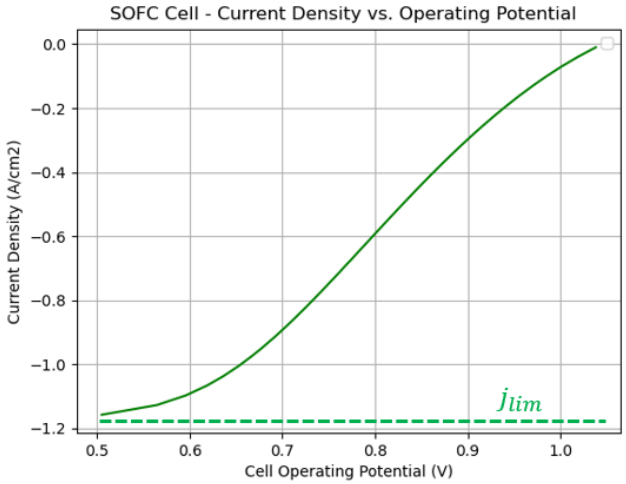

(a) SOEC cell J-V curve

Input Parameter	Numerical Value	Unit
p_{H_2}	0.9	[ ]
p_{H_2O}	0.1	[ ]
p_{O_2}	0.21	[ ]
T_{cell}	800	[°C]

(b) Input Parameters Values

Figure 12: SOEC cell J-V Characteristic Curves

3.2.3.2 SOFC Stack The electrical model of the Solid Oxide Fuel Cell Stack (SOFC), functions as a black box. Hydrogen and oxygen enter the stack at a designated temperature, denoted as T_{cell} and initially set at 800°C. The stack comprises multiple interconnected SOFC cells arranged in series, where the injected hydrogen and oxygen are distributed across the cells constituting the stack. Notably, a stack is composed of 130 SOFC cells linked in series. Electrochemical oxidation of the fuel takes place independently in each of these 130 SOFC cells, resulting in the production of H_2O and power under the form of electricity. The exit temperature of the H_2O gases is contingent upon the operational status of the individual cells. The decision to employ a stack with 130 cells

is based on insights derived from a prior scientific report [32], which extensively examined the cost and manufacturing aspects of a stack with the same cell count. It is important to note that all cells within a stack are considered to be operated at the same point on the J-V curve. Table 3 provides a summary of the key characteristics of the selected stack.

3.2.3.3 SOFC System The SOFC system model, depicted in Figure 13, operates as a sealed system. Hydrogen and oxygen enter under standard testing conditions, specifically at 25°C and atmospheric pressure. The water exiting the SOFC system is assumed to leave under standard testing conditions. The SOFC system produces electrical power P_{out} and produces heat $\dot{Q}_{out}$ as a byproduct of its operation. Within this sealed system, SOFC stacks are arranged in series along with the Balance of Plant (BOP). The BOP encompasses various components, including the heat model. As detailed in section 3.2.1, it's worth noting that the SOFC heat model requires further refinement, and therefore, $\dot{Q}_{out}$ is thus currently not taken into consideration in the BOP. However, it is crucial to bear in mind that the SOFC system incorporates the BOP when calculating the system's capital expenditure (CAPEX) costs in further sections.

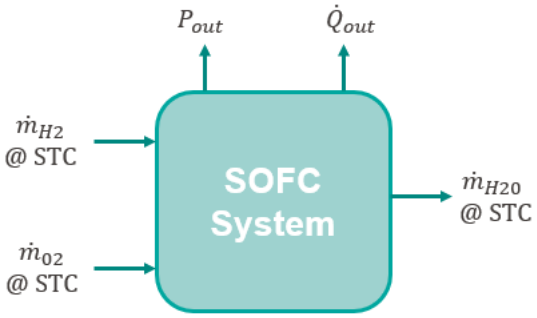

Figure 13: Overview SOFC system as black-box

System's Size Calculations: Unlike the SOFC stack, whose number of cells or size is predetermined, the number of SOFC stacks in series within the SOFC system is variable. The specific quantity of SOFC stacks in series within the SOFC system depends on both the cell current density J_{cell} at which all cells in all stacks operate and the hydrogen feed-in rate $\dot{m}_{H_2}$ for which the SOFC system is designed. To determine the number of SOFC stacks n_{stack} in series within the SOFC system for a fixed cell current density J_{cell} and hydrogen feed-in rate $\dot{m}_{H_2}$, the stack current I_{stack} is first calculated. The stack current represents the current consumed by each stack of the SOFC system under the specified conditions outlined in Figure 12b and for a specific cell current density J_{cell}.

$$I_{\text{stack}} = J_{\text{cell}} \cdot \frac{n_{cell}}{1 \text{ stack}} \cdot A_{\text{cell}} \tag{26}$$

in units of amperes [A].

Hydrogen oxidation at the anode releases electrons, contributing to the current in proportion to the hydrogen feed rate, as per Faraday's law. Consequently, the stack current (I_{stack}) not only defines the electrical output but also correlates with the hydrogen consumption rate per stack.

The hydrogen feed-in rate ($\dot{m}_{H_2}$) for the SOFC system sets the total hydrogen usage for all stacks. This rate is transformed into an electrical measure called the system current (I_{system}). The system current I_{system} represents the sum of all stack currents in the system I_{stack}.

$$I_{system} = \frac{\dot{m}_{H_2} \cdot r_{fuel,utilization}}{M_{H_2}} \cdot z \cdot F \tag{27}$$

in units of amperes [A].

To deduce the total number of SOFC stacks (n_{stack}) in the SOFC system, the following equation is employed:

$$n_{stack} = \frac{I_{system}}{I_{stack}} \tag{28}$$

This methodology offers a precise approach to ascertain the optimal number of stacks required for a specified system's hydrogen feed-in rate $\dot{m}_{H_2}$ and cell operating current density J_{cell} within an SOFC system.

System's Electrical Efficiency Calculations : The determination of the SOFC system's electrical efficiency involves parameters analyzed in distinct steps. Firstly, the power produced by the entire system P_{prod} is computed, using the cell current density J_{cell}, cell operating voltage E_{cell}, the number of cells in each stack $\frac{n_{cells}}{1 \text{ stack}}$, the cell active area A_{cell} and the number of stacks in the SOFC system n_{stacks} (see equation 3.2.3.3). This is expressed as

$$P_{\text{prod}} = J_{\text{cell}} \cdot E_{\text{cell}} \cdot \frac{n_{\text{cells}}}{1 \text{ stack}} \cdot n_{\text{stacks}} \cdot A_{cell} \tag{29}$$

in units of watts (W).

Subsequently, the total system's hydrogen consumption rate $\dot{m}_{\text{H}_{2,c}}$ is calculated, considering a fuel utilization rate $r_{fuel,utilization}$. Based on common industry knowledge and literature review, the fuel utilization rate $r_{fuel,utilization}$ is considered to be equal to 0.8 [36].

$$\dot{m}_{\text{H}_{2,c}} = \dot{m}_{\text{H}_2} \cdot r_{fuel,utilization} \tag{30}$$

in units of kilograms per second $[\frac{kg}{s}]$. In literature, hydrogen production rates are commonly expressed in $[W]$ using the higher heating value of hydrogen HHV_{H_2} to transition from $[\frac{kg}{s}]$ towards $[W]$.

Finally, the electrical efficiency of the entire SOFC system (η_{ele}) is computed using the equation

$$\eta_{\text{ele}} = \frac{P_{\text{prod}}}{\dot{m}_{\text{H}_{2,c}} \cdot HHV_{\text{H}_2}} \tag{31}$$

considering the higher heating value of hydrogen (HHV_{H_2}). This efficiency metric is dimensionless, quantifying the electrical efficiency while excluding the influence of input heat into the system, as mentioned in section 3.2.1.

Figure 9 illustrates how the electrical efficiency of the SOFC system varies with different cell current densities, denoted as J_{cell}. There is a noticeable downward trend in electrical efficiency as the cell

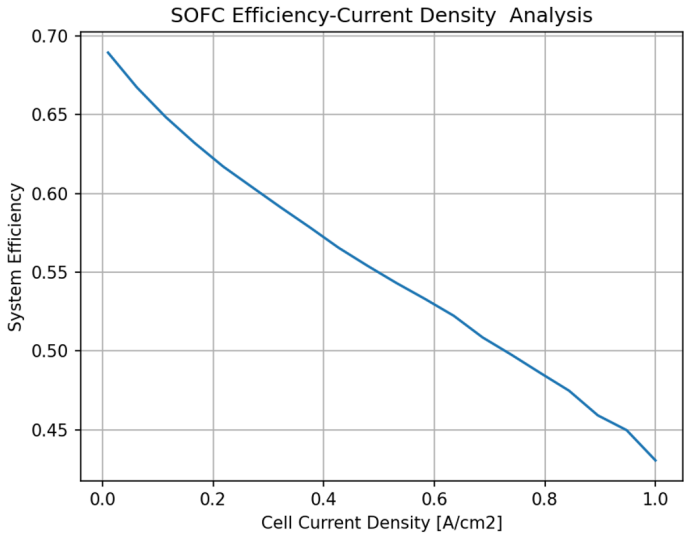

Figure 14: SOFC system's electrical efficiency versus cell current density

current density rises. The electrical efficiency values depicted on the y-axis correlate well with those reported in existing literature, as referenced in [37]. Additionally, it's important to highlight that the efficiency of a SOFC system can be enhanced through the utilization of waste heat in a combined heat and power (CHP) system.

System's Cost Calculations : The cost of the SOFC system is primarily determined by two factors: the cost of the SOFC stacks and the Balance of Plant (BOP) cost. While further refinement is still needed for the heat model, it is however already possible to incorporate the Balance of Plant (BOP) costs in the current analysis. The SOFC system's capital expenditure (capex) cost is computed in the exact same way as for the SOEC system, as discussed in section 3.2.2.3

As a reminder, accounting for both BOP and SOFC costs, the total SOFC system's capex cost $Capex_{\text{tot, SOFC}}$ is computed as:

$$Capex_{\text{tot, SOFC}} = 2 \cdot Capex_{\text{system, SOFC}} \tag{32}$$

in units of dollars [$].

Figure 15 illustrates the total capex cost of the SOEC system across different cell current densities J_{cell}. The trend indicates a decrease in total cost with an increase in cell current density as the number of stacks in the SOEC system n_{stacks} decreases.

Cost Efficiency Dilemma : Figure 16 presents the relationship between the electrical efficiency of the SOFC system and its total capex cost. A dilemma becomes evident, as operating at higher electrical efficiency results in a higher total capex cost for the SOFC system, while lower electrical efficiencies correspond to lower total costs. It is important to note that each point along the curve in Figure 16 corresponds to a specific cell current density J_{cell}.

In conclusion, a dilemma arises between the electrical efficiency of the SOFC system and its total system cost. Additionally, it has been demonstrated that the cell current density at which the

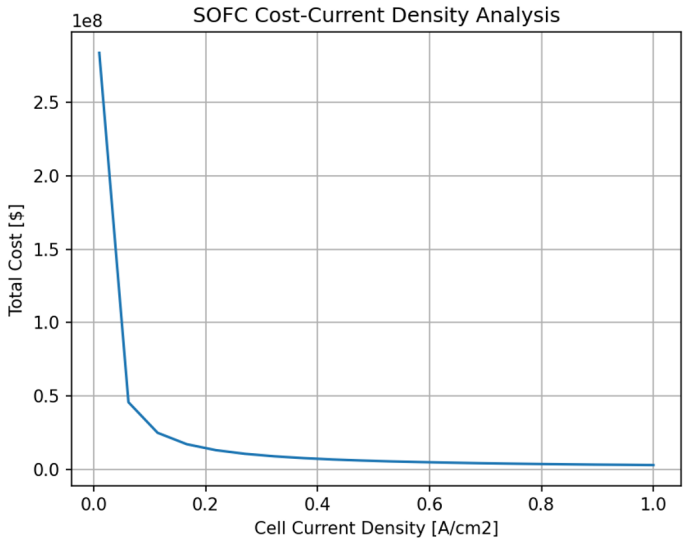

Figure 15: Total SOFC system's cost versus cell current density

SOFC cells operate significantly influences the total cost of the SOFC system and its electrical efficiency.

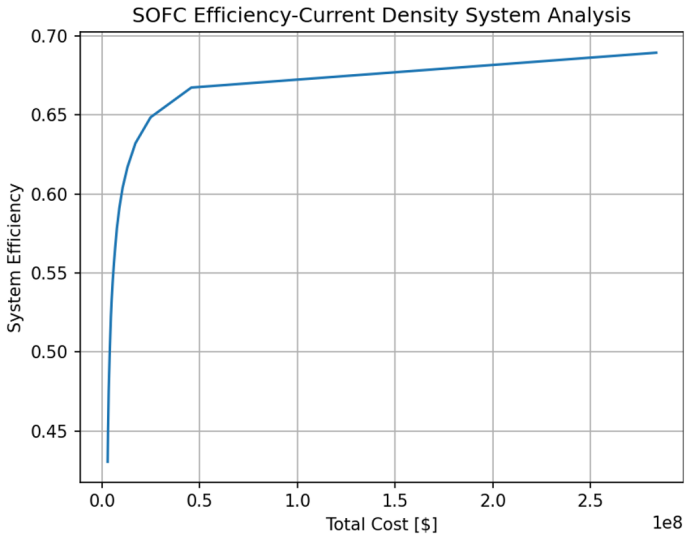

Figure 16: SOFC system's efficiency versus Total SOFC system's cost

3.2.4 Storage System

Following the examination of SOEC and SOFC systems, attention will now be directed towards the storage system as illustrated in Figure 3. In the context of researching the use of Solid Oxide Fuel Cells (SOFC) and Solid Oxide Electrolyzer Cells (SOEC) for long-term electrical energy storage systems, understanding the nuances of hydrogen storage is crucial. Hydrogen serves as a key element in these systems, both as a fuel and a storage medium. Its storage, however, presents several challenges and opportunities, especially in terms of energy requirements and system efficiency as

previously briefly discussed in section 3.1.3.

3.2.4.1 Introduction to hydrogen storage technologies

Hydrogen can be stored in two primary physical forms: as compressed gas (GH2) at high pressures (350 to 700 bar) and as liquid hydrogen (LH2). Consequently, the hydrogen storage model has been developed to function with both potential physical forms of hydrogen, specifically liquid hydrogen (LH2) and gaseous hydrogen (GH2). The energy requirements for these storage methods are significant and vary based on the chosen storage method. Compressing hydrogen from 20 bar to 350 or 700 bar requires 1.05 and 1.36 kWh/kg H2 respectively, in theory, but practical scenarios, including compressor inefficiencies and rapid filling processes, increase this demand substantially, ranging from 1.7 to 6.4 kWh/kg H2 as per the DOE Technology Validation Project data [38]. Additional energy is required for pre-cooling under GH2-storage, which can be around 0.15 kWh/kg H2, to maintain onboard temperatures during fast fills [39].

On the other hand, the liquefaction of hydrogen, which involves cooling it to a liquid state, requires a minimum of 3.3 kWh/kg LH2 or 3.9 kWh/kg LH2 when converting to para-LH2 (a common practice). Practical energy requirements for this process are higher, typically between 10-13 kWh/kg LH2, influenced by the scale of the operation [38]. Novel methods such as active magnetic regenerative liquefiers may lower this to around 7 kWh/kg LH2 [40].

For both storage methods, the energy required is a significant portion of the lower heating value (LHV) of hydrogen (33.3 kWh/kg H2), with compression using about 5 - 20% and liquefaction 30 - 40% of the LHV [38]. These figures highlight the importance of optimizing the storage method for maximum efficiency in long-term energy storage systems through hydrogen.

The types of compressors used for hydrogen storage also play a critical role. Common types include positive displacement compressors (reciprocating or rotary) and centrifugal compressors [41]. Each type has its advantages, with reciprocating compressors being more suitable for high compression ratios and centrifugal compressors preferred for pipeline applications due to their high throughput. Innovative alternatives like ionic compressors and electrochemical compressors are also under exploration for their potential efficiencies and lower failure rates [41].

3.2.4.2 Conception of the hydrogen storage model

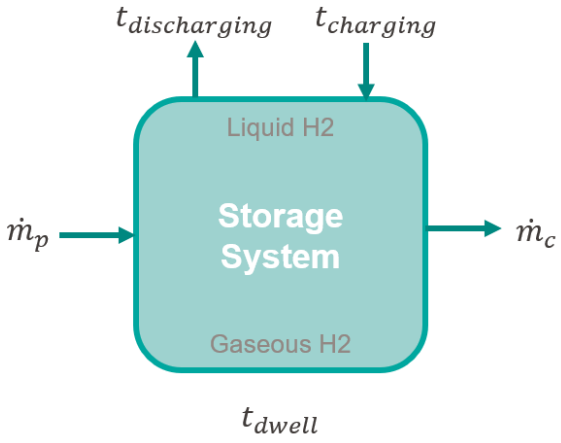

Figure 17: Hydrogen storage system

Storage Model Parameter	Value	Units
$t_{discharging}$	-	[day]
$t_{charging}$	-	[day]
t_{dwell}	-	[day]
Hydrogen output rate $\dot{m}_c$	-	[W]
Hydrogen input rate $\dot{m}_p$	-	[W]

Figure 18: Hydrogen storage parameters

The model has been designed to operate as a black-box system. Hydrogen is introduced into the storage system at a specific rate denoted as $\dot{m}_p$, which typically corresponds to the hydrogen production rate of the Solid Oxide Electrolysis Cell (SOEC) system. This input rate is maintained for a duration of $t_{charging}$. Subsequently, the accumulated hydrogen is converted into the storage form, either gaseous hydrogen (GH2) or liquid hydrogen (LH2), and stored for a period of t_{dwell}. Following the storage phase, the stored hydrogen is released, typically directed towards the Solid Oxide Fuel Cell (SOFC) system, at a designated output rate $\dot{m}_c$ for a duration equal to $t_{discharging}$.

It is important to note that, considering the model's final application, the variables $t_{charging}$ and $t_{discharging}$ are defined within the SOEC and SOFC models, respectively. Specifically, it is assumed that $t_{charging}$ corresponds to the duration during which the SOEC system operates, as all produced hydrogen is directed towards storage during this period. Conversely, $t_{discharging}$ is defined as the operation time of the SOFC system, as all hydrogen released from the storage tank is used directly to operate the SOFC system.

As mentioned in section 3.2.4.1, the hydrogen storage model has been developed to function with both potential physical forms of hydrogen storage, namely (LH2 and GH2).

3.2.4.3 Liquid Hydrogen Storage - LH2

Storage Model Parameter	Value	Units
Tank Storage Temperature	20	[K]
Boil-off rates	0.2	$[\frac{\%}{\text{day}}]$

Table 4: Overview of parameters specific to liquid hydrogen storage

Empirical measurements obtained from real-scale liquefiers have been favored over theoretical formulas due to observed discrepancies between theoretical models and real-scale liquefiers. These measurements are derived from reports published by the United States Department of Energy in 2019 [38]. These reports comprehensively analyzed the costs and energy requirements associated with hydrogen liquefaction, specifically for hydrogen storage with an emphasis on energy storage applications.

Storage Losses : Boil-off rates in liquid hydrogen storage systems refer to the rate at which stored hydrogen transitions from a liquid state to a gaseous state due to the natural tendency of hydrogen to evaporate under such conditions. This phenomenon occurs when the storage conditions, such as temperature and pressure, are not perfectly controlled. Boil-off rates are a critical consideration in hydrogen storage systems, as they impact the efficiency and safety of the storage process. Reducing boil-off rates is important to minimize hydrogen losses and optimize the performance of the storage system.

To calculate the hydrogen output rate ($\dot{m}_c$) while considering boil-off rates :

$$\dot{m}_c = (1 - r_{boil-off} \cdot t_{dwell}) \cdot \dot{m}_p \tag{33}$$

in units of watts [W].

Capital of Expenditure : Figure 19a illustrates the results of the empirical analysis applied to capital expenditure. The reports in use [38] quantify the capital expenditure for liquefaction

equipment based on the liquefied hydrogen's capacity, measured in megawatts (MW). This 'liquefied capacity' specifically refers to the hydrogen liquefaction rate. It's worth noting that the capital expenditure (capex) depicted in this figure only covers the upfront cost of acquiring the liquefaction equipment itself. It doesn't take into account the tank cost, expenses related to purchasing electricity from the grid to operate the liquefier or any maintenance and operational costs. The collected data points were subjected to polynomial regression to achieve a fitted curve.

Figure 19b provides insight into the capital expenditure (capex) cost per kilogram of liquefied hydrogen. When we compare figure 19a and figure 19b, an interesting contrast emerges. While the total capex cost does indeed rise with greater liquefier capacity, there's a noteworthy inverse relationship when we consider the capex cost per kilogram of hydrogen liquefied. As liquefier capacity increases, the capex cost per kilogram of hydrogen liquefied decreases.

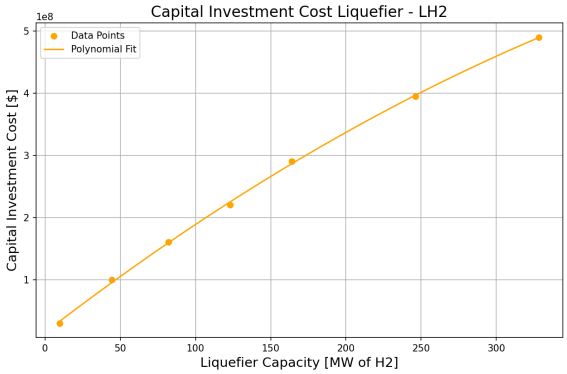

(a) Capital expenditure for liquefiers of different capacities

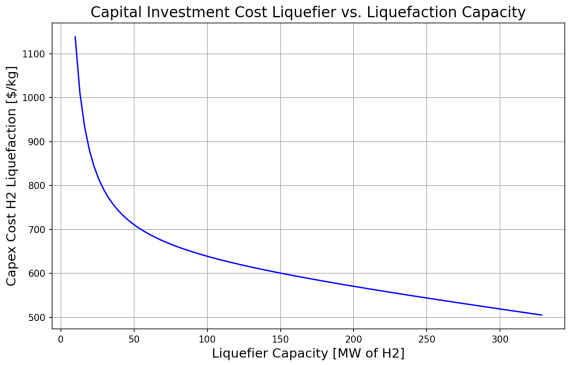

(b) Capital expenditure per kilogram for various liquefier capacities

Figure 19: Capital expenditure per kilogram for various liquefier capacities

With the capital expenditure for liquefiers now established, the subsequent step involves determining the cost of the cryogenic tank to ascertain the total capital expenditure for the liquid hydrogen storage system.

According to the "Hydrogen Storage Cost Analysis" (2022) [42], the average cost of a cryogenic hydrogen storage tank is 31.60 $[\frac{\$}{\text{kg}}]$. Note that this figure is an average and the actual cryogenic tank's capital expenditure ($Capex_{tank}$) can vary significantly due to factors such as material costs, manufacturing complexities, and market conditions. The cryogenic tank's capital expenditure, $Capex_{tank}$, based on the tank's hydrogen capacity $m_{H_2\_tank}$, is calculated as:

$$m_{H_2,tank} = \frac{\dot{m}_c}{HHV_{H_2}} \cdot t_{charging} \tag{34}$$

in units of kilogram [kg].

$$Capex_{tank} = 31.60[\frac{\$}{\text{kg}}] \cdot m_{H_2,tank} \tag{35}$$

in units of dollars [$].

The total capital expenditure (capex) for the liquid hydrogen storage system $Capex_{LH2,system}$, is

formulated as :

$$Capex_{LH2,system} = Capex_{tank} + Capex_{liquefier} \tag{36}$$

in units of dollars [$].

Energy Requirements : As previously mentioned the liquefaction of hydrogen, which involves cooling it to a liquid state, requires a minimum of 3.3 kWh/kg LH2 or 3.9 kWh/kg LH2 when converting to para-LH2 (a common practice). However practical energy requirements for this process are higher, typically between 10-13 kWh/kg LH2, influenced by the scale of the operation [38]. The collected data points were subjected to polynomial regression to achieve a fitted curve. One can observe that as the liquefier capacity increases, the liquefaction energy requirement per kilogram of hydrogen for liquefaction decreases.

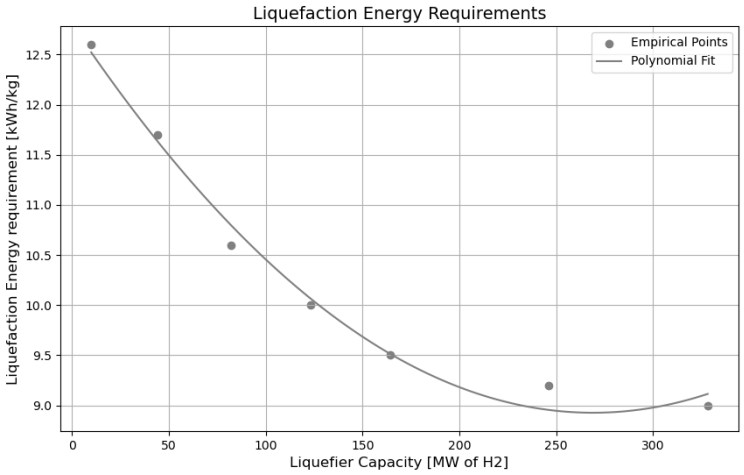

Figure 20: Hydrogen liquefication energy requirements

3.2.4.4 Gaseous Hydrogen Storage - GH2

Storage Model Parameter	Value	Units
Storage Pressure $p_{H_2,out}$	500	[bar]

Table 5: Overview of parameters specific to gaseous hydrogen storage

In the design of hydrogen storage systems, the selection of a gaseous hydrogen tank with a storage pressure $p_{H_2,out}$ of 500 bar represents a strategic decision balancing efficiency, safety, and economic factors [43]. This high-pressure threshold is primarily chosen to maximize storage capacity. At 500 bar, hydrogen's density increases significantly, allowing for a larger amount of hydrogen to be stored in a comparably smaller volume, thereby enhancing the storage efficiency.

Moreover, the choice of 500 bar, a pressure level that is technically feasible and widely used in the industry, strikes a balance between achieving high storage density and maintaining manageable material and operational costs [44]. Tanks designed to withstand such pressures are constructed using advanced materials and engineering techniques to ensure safety and durability, yet they remain economically viable.

Furthermore, the infrastructure for refueling and handling hydrogen at this pressure level is relatively more developed and accessible, compared to higher pressures like 700 bar or lower pressures where storage efficiency is significantly reduced. This compatibility with existing infrastructure eases integration challenges and supports broader adoption of hydrogen technologies.

Storage losses : For the gaseous hydrogen storage model, it is assumed that losses during storage are negligible. Therefore, the hydrogen output rate $\dot{m}_c$ equals the hydrogen input rate $\dot{m}_p$.

Capital of Expenditure : An empirical formula has been used to calculate the capital expenditure related to acquiring a GH2 storage system.

$$Capex = 220800 + 366.7 \cdot \frac{E_{compr}}{t_{charging}} \tag{37}$$

Energy Requirements : To estimate the energy needed to compress hydrogen to an elevated pressure p_{H_2out}, the compression process is idealized as isothermal and the hydrogen gas is treated as an ideal gas. This approach is widely accepted and employed in academic research, including the methodologies used in Professor Andreas Züttel's LMER laboratory [45].

Assuming isothermal compression and ideal gas and :

- $k = 1.410$ (at 293K)
- $T = 298$ K
- $\eta_{\text{compr}} = 0.7$

$$E_{\text{compr}} = \frac{\frac{k}{k-1} \cdot R \cdot T \cdot \left[\left(\frac{P_{H2,\text{out}}}{P_{H2,\text{in}}} \right)^{\frac{k}{k-1}} - 1 \right]}{\eta_{\text{compr}} \cdot M_{H2}} \cdot t_{\text{charging}} \cdot \dot{m}_p \tag{38}$$

in units of [kWh].

To validate the outcomes derived from equation 3.2.4.4, the calculated values were juxtaposed with empirical data from Professor Züttel's laboratory. Utilizing the standard parameter values outlined in table 5, the computation yielded an energy requirement for hydrogen compression relative to its Higher Heating Value (HHV), denoted as $\frac{W}{HHV}$, amounting to 6.6%. This figure was then compared to the data illustrated by the blue curve in figure 21, which represents the same ratio for isothermal compression of hydrogen. The close alignment of our theoretical model's result of 6.6% with this empirical data serves to corroborate the accuracy and reliability of the theoretical formula utilized.

3.2.5 Results

Having explored the Solid Oxide Electrolyzer Cell (SOEC) and Solid Oxide Fuel Cell (SOFC) system models, along with the storage system, the next step is to integrate these two models, as illustrated in Figure 3.

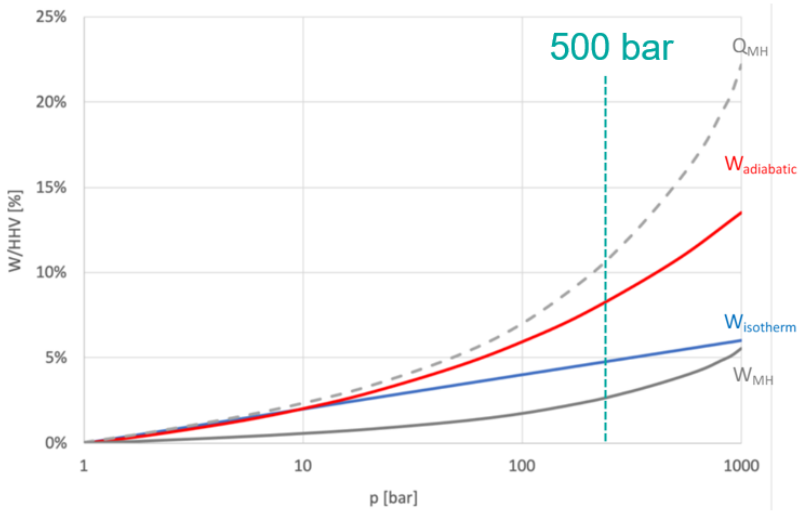

Figure 21: Hydrogen compression energy requirement, adapted from Züttel's lecture on Hydrogen Storage (2023) [45]

The primary objective of this report is to calculate the overall efficiency of the system that converts electricity to hydrogen (either liquefied or gaseous) and back to electricity. This comprehensive efficiency, denoted as $\eta_{elec,tot}$, is determined using the output power of the SOFC system (P_{out}), the operating duration during discharge ($t_{discharging}$), the input power to the SOEC system (P_{in}), the operating duration during charging ($t_{charging}$), and the energy required for hydrogen liquefaction or compression (E_{compr}). The formula for calculating the total electrical efficiency is given by:

$$\eta_{elec,tot} = \frac{P_{out} \cdot t_{discharging}}{P_{in} \cdot t_{charging} + E_{compr}} \tag{39}$$

Considering the aforementioned details, one example has been selected to demonstrate the functionality of the model and to clearly illustrate how it operates.

Figure 22 illustrates a hydrogen storage system tailored for a 2MW input power from the grid. In this configuration, the Solid Oxide Electrolyzer Cell (SOEC) is operational for a $t_{charging}$ period of 4 days, during which hydrogen is produced. This hydrogen is then stored in liquid form within a cryogenic tank for a dwelling time, t_{dwell}, of 166 days. The selection of a 166-day dwelling period is intentional, as this Power-to-Hydrogen-to-Power (PtH2tP) system is specifically designed for long-term energy storage. The 166 days, representing approximately half a year, aligns with the concept of storing surplus electricity generated during the Swiss summer and then redistributing this stored energy during the winter months. Following the storage phase, the stored hydrogen is planned to be deployed through a Solid Oxide Fuel Cell (SOFC) system over a discharging period, $t_{discharging}$ of 4 days, allowing to inject an output power P_{out} into the grid. This example is provided mainly to elucidate and demonstrate the model's final outputs in a practical scenario.

The results depicted in Figure 22 are specific to an operating current density of $J_{cell} = 0.5\frac{A}{cm^2}$. To expand upon these findings, the total system efficiency of the system presented in Figure 22 has been calculated across a range of cell operating current densities, J_{cell}. This analysis, depicted in Figure 23, emphasizes the critical role that the cell's current density plays in determining the total efficiency of the system.

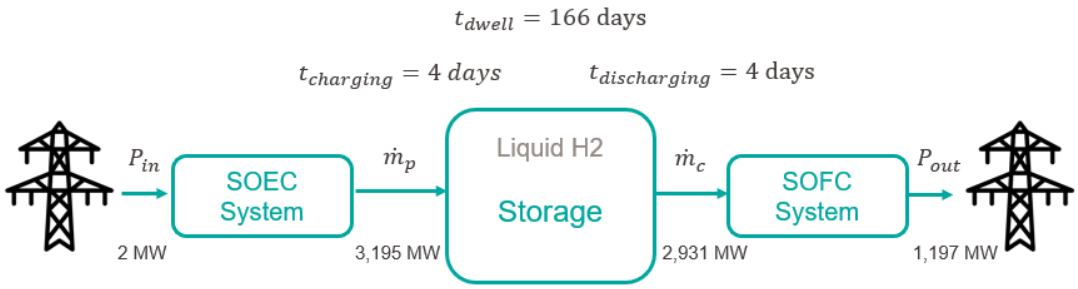

	SOEC	Storage	SOFC	Total
Cost	7,992 M $	21,1 M $	5,904 M $	35,0M
Efficiency	1.59		0.511	0.394
I_{cell}	0.5 $\frac{A}{cm2}$		0.5 $\frac{A}{cm2}$	0.5 $\frac{A}{cm2}$

Figure 22: Main outcomes of the power-to-H_2-tank-to-power model for a defined variable set

To expand upon these findings, the total system cost of the system presented in Figure 22 has been calculated across a range of cell operating current densities, J_{cell}. In order to have a better overview of the SOEC, SOFC and storage system's cost figure 24 showcases each of those subcosts with varying cell current densities. It is important to exercise caution when interpreting Figure 24, due to the utilization of differing scales on the two y-axes.

Finally, both the total system efficiency and total system cost are compared within one graph in Figure 25.

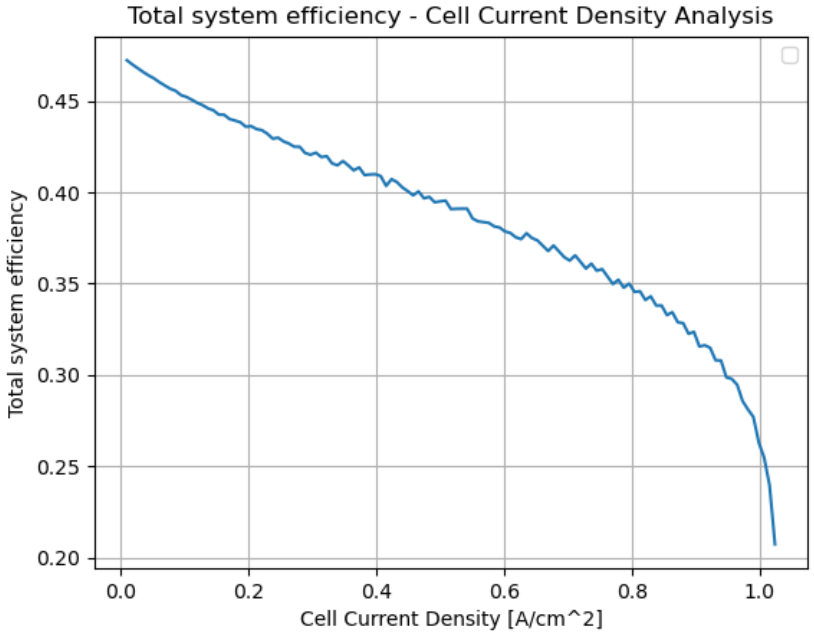

Figure 23: Total system's efficiency of the power-to-H_2-tank-to-power model for a defined variable set while varying the cell current density J_{cell}

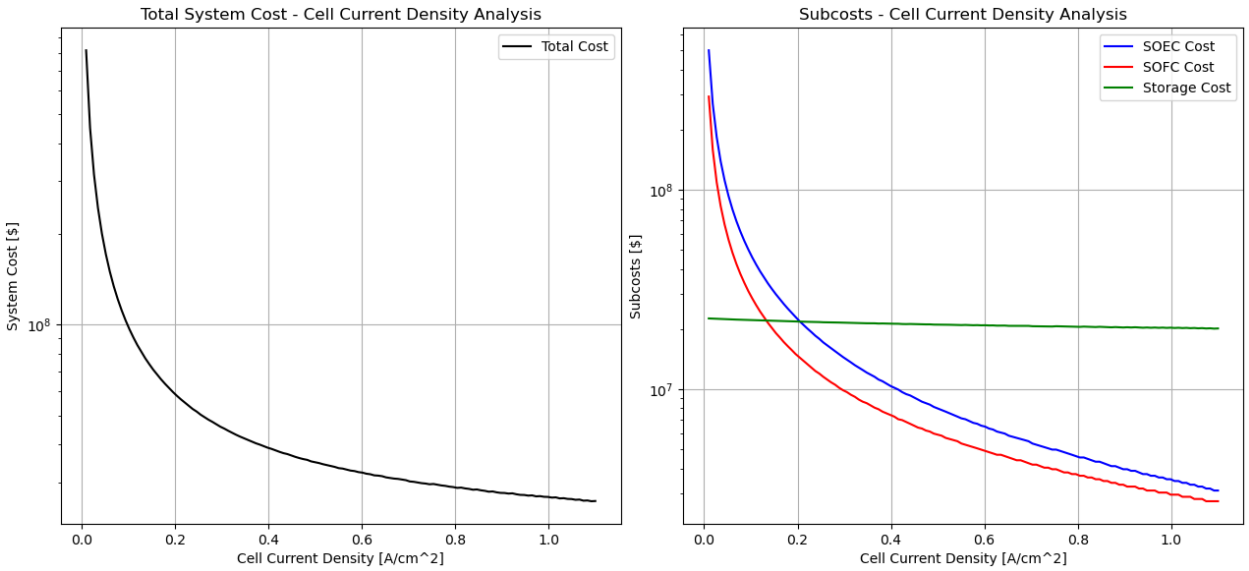

Figure 24: Total system's cost of the power-to-H_2-tank-to-power model for a defined variable set while varying the cell current density J_{cell}

3.2.5.1 Discussion of obtained results

Reviewing the total system efficiency (Figure 23), it is evident that efficiency decreases with an increase in cell current density, staying within a 20% to 50% range. A significant efficiency reduction is apparent at 1.1 $\frac{A}{cm^2}$, aligning with the limiting current density effect due to mass transport limitations, as explored in sections 3.2.2.1 and 3.2.3.1.

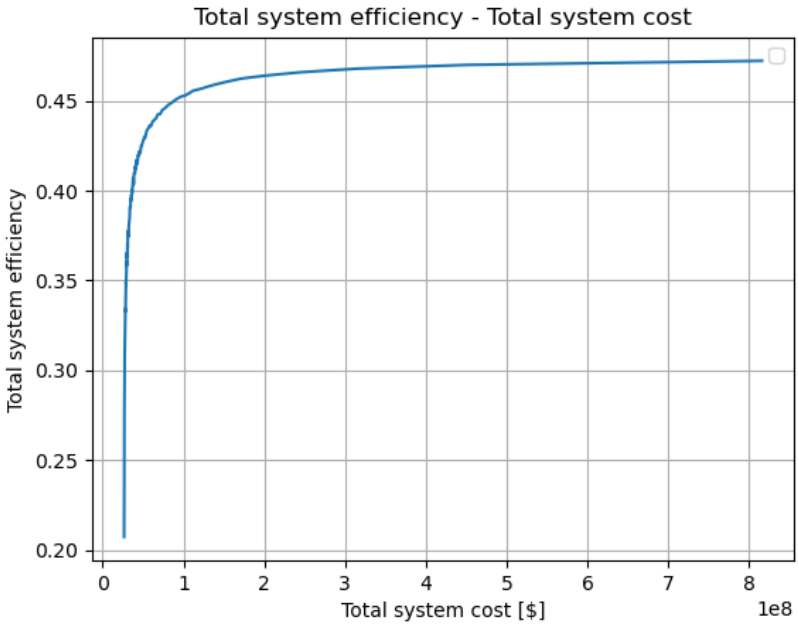

Figure 25: Total system's efficiency versus total systems cost of the power-to-H_2-tank-to-power model

In terms of costs, as depicted in Figure 24, the total system cost shows a downward trend as cell current density goes up, indicating fewer stacks are needed. Costs vary between 900 million and 9.4 million dollars. The peak cost of 900 million dollars is linked to very low cell current densities, which are generally not operational for SOEC and SOFC cells. Examining the subcosts reveals that storage cost starts to predominate over SOEC and SOFC costs beyond a cell current density of 0.2 A/cm². While the costs associated with SOEC and SOFC systems show a decrease as the current density increases, the reduction in the storage costs is not as pronounced as in the case of SOEC and SOFC systems. Finally, the total system cost falls mostly as cell current density increases due to decreasing SOEC and SOFC system costs.

Finally, when comparing total system efficiency versus total system cost of the power-to-H_2-tank-to-power model (Figure 25), the usual dilemma between efficiency and capex cost can be noticed again as for the case of SOEC (section 3.2.3.3) and SOFC systems (section 3.2.2.3).

3.2.5.2 Validation of obtained results

Cost validation : To validate the cost estimates obtained for the SOEC and SOFC systems as depicted in Figure 22, a comparative analysis was conducted with an existing installation in Switzerland. Specifically, the model's cost projections were compared with those of a 2-MW electrolysis facility operated by GroupE, located near a dam in the canton of Fribourg, as of August 2023 [46]. The calculated capital expenditures (capex) closely align with the Fribourg installation's cost of 9.14 million USD. The observed discrepancy of about 1 million USD between the model's estimates and the actual costs of the Fribourg project could be attributed to various factors. For instance, the Fribourg project being a trailblazer in the field might have incurred unique expenses, or the model's cost assumptions that have been based on projected electrolyzer and fuel cell costs anticipated for the year 2030.

Efficiency validation : So far, the analysis has focused solely on the electrical efficiency of the systems, excluding any consideration of heat inputs and outputs. Locating specific values of electrical efficiency in existing literature has proven challenging, making it difficult to externally validate the efficiencies calculated for various sets of variables. Despite this, the accuracy of these values is supported by the confirmation and approval of other members from the IPESE lab, suggesting that the obtained efficiency figures are likely correct.

3.3 Heat Model

As highlighted in section 3.1, the focus has been placed on developing the electrical model, leaving the heat model in need of further refinement. The subsequent section addresses the necessity of such a heat model.

The Solid Oxide Electrolyzer Cell (SOEC) system, as depicted in Figure 3, requires input heat, denoted as $\dot{Q}in$. This heat serves two primary purposes: firstly, it heats the water to the SOEC cell's operational temperature, typically around 800°C; secondly, it facilitates the chemical reactions within the SOEC cell. The quantity of input heat $\dot{Q}in$ required varies depending on the SOEC cell's operating point.

Conversely, the Solid Oxide Fuel Cell (SOFC) system, also shown in Figure 3, produces output heat, indicated as $\dot{Q}out$. While this output heat is generally a positive value, the SOFC system still

necessitates some input heat to raise the temperature of hydrogen and oxygen to the cell's operating temperature, around 800°C. However, the heat generated by the SOFC during its electrochemical reaction typically exceeds the input heat needed to raise the temperature of hydrogen and oxygen. This output heat can be utilized for other industrial applications requiring high-temperature heat, or it can be converted back to electricity using heat pumps. It is important to note that the input heat required for preheating hydrogen and air is considerably less than the heat output by the SOFC system. Therefore, the focus is primarily on using the heat output, $\dot{Q}out$. The amount of heat generated varies with the operating point of the SOFC cell.

For an overview of the current status of heat models developed in Aspen, please refer to the appendix section A as depicted in Figure 26.

4 Areas of weakness

In the interest of thoroughness and continuous improvement, it is essential to acknowledge and discuss the current limitations and areas where the model may fall short. This section aims to candidly outline these aspects, providing a clear understanding of the model's weaknesses.

- **Specificity to Cell Type:** As outlined in section 3.2.2.1, the model is tailored to a specific type of SOEC/SOFC cell with unique characteristics like materials. Default values are set based on this specific cell type ([31]), which should be considered when interpreting results.
- **Fixed Input Power Assumption:** The model, as shown in Figure 3, assumes a constant input power (P_{in}). However, in practical scenarios where excess electricity is used for storage, the power received from the grid may vary.
- **Variability in Stack Cell Count:** The model's assumption that each SOEC or SOFC stack contains exactly 130 cells might not accurately reflect real-world variations. The number of cells per stack can vary significantly depending on the cell type and manufacturer's design.
- **Separate SOEC and SOFC Systems:** The current model features distinct SOEC and SOFC systems for electrolysis and electrochemical oxidation, respectively. In industrial settings, a single reversible system is often used for both functions to reduce costs.
- **Exclusion of Heat Considerations:** The model does not include heat dynamics, a critical factor in analyzing SOEC and SOFC performance.
- **Gaseous Hydrogen Storage System Accuracy:** While the model accurately estimates the energy required for hydrogen compression, the cost evaluation for compressors may require further verification or revision.

5 Recommendations for Future Research

This section is intended as a compilation of potential future endeavors that could be pursued using the developed model.

- **Comparison with P-to-Heat-to-Power Model:** Upon completion of the model, a primary task is to compare the Power-to-Hydrogen-tank-to-Power (PtH2tP) with the previously developed Power-to-Heat-to-Power (PtQtP) model as discussed in section 1.2. This

comparison should focus on efficiency and capital expenditure (capex) costs of both storage technologies.

- **Development of Additional Storage Models:** Future efforts could involve developing models for other existing storage technologies suitable for long-term electricity storage. Examples include Power-to-Methane-to-Power and Power-to-Battery-to-Power (PtBtP) systems.
- **Integration of Grid Dynamics:** With multiple Power-to-X-to-Power (PtXtP) models developed, integrating the electricity grid into these models can provide insights into optimal usage times based on grid electricity prices. This integration would allow for a cost comparison of various storage technologies against the backdrop of electricity price fluctuations.
- **Utilization of SOFC Heat Output:** In the Power-to-Hydrogen-tank-to-Power model, the heat output from the SOFC system could be harnessed. Parts of the existing Power-to-Heat-to-Power model could serve as a foundation for such an extension.
- **Experimental Validation of J-V Curve:** The J-V curves modeled within the SOEC and SOFC systems should be validated against experimental stacks to enhance the model's accuracy.
- **Revisiting Model Assumptions:** Addressing and refining the stated assumptions in the model is crucial for improving its precision and applicability.

6 Paper contribution

This report represents a collaborative effort involving Yi Zhao, a Ph.D. candidate at the IPESE lab from EPFL, and Jingjing Liang, a visiting Ph.D. scholar at the same lab. Among various accomplishments, the findings of this study have been submitted to the 37th International Conference on Efficiency, Cost, Optimization, Simulation, and Environmental Impact of Energy Systems (ECOS 2024).

7 Conclusion and Improvements

In concluding this semester project, we have delved into the intricacies of the Power-to-Hydrogen-Tank-to-Power (PtH2tP) system, exploring both its theoretical underpinnings and practical implications. The developed model output focuses on 2 key aspects when comparing various storage technologies being capital of expenditure and electrical efficiency. Noteworthy the heat model is not accounted for currently and only electrical efficiency has been computed.

When looking at the model and its parameters 5 key parameters can be identified being power input P_{in} from the grid, the charging time $t_{charging}$, the discharging time $t_{discharging}$, the dwelling time t_{dwell} and finally cell operating current density J_{cell}.

Finally when analyzing the entire modeled system. It can be seen that the total system efficiency and capex cost decrease with increasing cell current density. When comparing both total system electrical efficiency and capex cost a dilemma occurs as operating at higher electrical efficiency results in a higher total capex cost for the total system, while lower electrical efficiencies correspond to lower total costs.

When analyzing the total system costs components from closer it can be noticed that cost of the storage system decreases very few with the cell current density. At low cell current densities the SOFC and SOEC systems component are the dominant cost as more stacks are required at low cell current densities. However at higher cell current densities the storage system cost becomes the dominant cost component.

References

[1] Hannah Ritchie, Max Roser, and Pablo Rosado. "CO and Greenhouse Gas Emissions." In: *Our World in Data* (May 11, 2020). URL: https://ourworldindata.org/co2/country/switzerland (visited on 12/28/2023).

[2] Federal Office for the Environment FOEN. *Long-term climate strategy to 2050.* URL: https://www.bafu.admin.ch/bafu/en/home/themen/thema-klima/klimawandel-stoppen-und%20-folgen%20-meistern/%20massnahmen-der-schweiz-zur-verminderung-ihrer-treibhausgasemissionen/ziele-der-schweiz-zur-verminderung-ihrer-treibhausgasemissionen/%20indikatives-ziel-205 langfristige-klimastrategie-2050.html (visited on 12/28/2023).

[3] *Energy – Facts and Figures.* URL: https://www.eda.admin.ch/aboutswitzerland/en/home/wirtschaft/energie/energie---fakten-und-zahlen.html (visited on 12/28/2023).

[4] *New study: Energy Future 2050 - Security of supply and climate neutrality by 2050.* URL: https://www.admin.ch/gov/en/start/documentation/media-releases.msg-id-92180.html (visited on 12/28/2023).

[5] Marta Victoria et al. "Solar photovoltaics is ready to power a sustainable future." In: *Joule* 5.5 (May 19, 2021), pp. 1041–1056. URL: https://www.sciencedirect.com/science/article/pii/S2542435121001008 (visited on 12/28/2023).

[6] Romain Phan. "The optimal Power-to-X-to-Power." In: (2023), pp. 1–43.

[7] Gunther Glenk and Stefan Reichelstein. "Economics of converting renewable power to hydrogen." In: *Nature Energy* 4.3 (Mar. 2019). Number: 3 Publisher: Nature Publishing Group, pp. 216–222. URL: https://www.nature.com/articles/s41560-019-0326-1 (visited on 12/28/2023).

[8] Saheli Biswas et al. "A Review on Synthesis of Methane as a Pathway for Renewable Energy Storage With a Focus on Solid Oxide Electrolytic Cell-Based Processes." In: *Frontiers in Energy Research* 8 (2020). URL: https://www.frontiersin.org/articles/10.3389/fenrg.2020.570112 (visited on 12/28/2023).

[9] M. J. Bos, S. R. A. Kersten, and D. W. F. Brilman. "Wind power to methanol: Renewable methanol production using electricity, electrolysis of water and CO2 air capture." In: *Applied Energy* 264 (Apr. 15, 2020), p. 114672. URL: https://www.sciencedirect.com/science/article/pii/S0306261920301847 (visited on 12/28/2023).

[10] *Switching to hydrogen fuel could prolong the methane problem.* Andlinger Center for Energy and the Environment. Mar. 13, 2023. URL: https://acee.princeton.edu/acee-news/switching-to-hydrogen-fuel-could-prolong-the-methane-problem/ (visited on 12/28/2023).

[11] D. S. Falcão and A. M. F. R. Pinto. "A review on PEM electrolyzer modelling: Guidelines for beginners." en. In: *Journal of Cleaner Production* 261 (July 2020), p. 121184. URL: https://www.sciencedirect.com/science/article/pii/S0959652620312312 (visited on 11/15/2022).

[12] Andre Leonide, Yannick Apel, and Ellen Ivers-Tiffee. "SOFC Modeling and Parameter Identification by Means of Impedance Spectroscopy." en. In: *ECS Transactions* 19.20 (Oct. 2009). Publisher: IOP Publishing, p. 81. URL: https://iopscience.iop.org/article/10.1149/1.3247567/meta (visited on 11/29/2022).

[13] Dino Klotz et al. "Current-Voltage and Temperature Characteristics of Anode Supported Solid Oxide Electrolyzer Cells (SOEC)." en. In: *ECS Transactions* 45.1 (Apr. 2012). Publisher: IOP Publishing, p. 523. URL: https://iopscience.iop.org/article/10.1149/1.3701344/meta (visited on 11/29/2022).

[14] Vikram Menon, Vinod M. Janardhanan, and Olaf Deutschmann. "A mathematical model to

analyze solid oxide electrolyzer cells (SOECs) for hydrogen production." In: *Chemical Engineering Science*. Mackie-2013 "Pushing the boundaries" 110 (May 3, 2014), pp. 83–93. URL: https://www.sciencedirect.com/science/article/pii/S0009250913007124 (visited on 01/27/2024).

[15] Liming Ba et al. "A study on solid oxide electrolyzer stack and system performance based on alternative mapping models." In: *International Journal of Hydrogen Energy* 47.25 (Mar. 22, 2022), pp. 12469–12486. URL: https://www.sciencedirect.com/science/article/pii/S0360319922004979 (visited on 01/27/2024).

[16] Christoph Meier et al. "Lagrangian model using CFD flow data to predict the current-voltage characteristics of a solid oxide fuel cell repeat unit." In: *The International Journal of Multiphysics* 12.4 (2018). Accepted: 2018-12-21T15:04:45Z Publisher: International Society of Multiphysics, pp. 393–411. URL: https://digitalcollection.zhaw.ch/handle/11475/14148 (visited on 01/27/2024).

[17] Fiammetta Rita Bianchi et al. "Multiscale Modeling for Reversible Solid Oxide Cell Operation." In: *Energies* 13.19 (Jan. 2020). Number: 19 Publisher: Multidisciplinary Digital Publishing Institute, p. 5058. URL: https://www.mdpi.com/1996-1073/13/19/5058 (visited on 01/27/2024).

[18] *Correlation between hydrogen production rate, current, and electrode overpotential in a solid oxide electrolysis cell with La0.6Sr0.4FeO32d thin-film cathode*. URL: https://www.google.com/search?q=Correlation+between+hydrogen+production+rate%2C+current%2C+and+electrode+overpotential+in+a+solid+oxide+electrolysis+cell+with+La0.6Sr0.4FeO32d+thin-film+cathode (visited on 01/27/2024).

[19] *Hydrogen production through steam electrolysis: Model-based dynamic behaviour of a cathode-supported intermediate temperature solid oxide electrolysis cell - Recherche Google*. URL: https://www.google.com/search?q=Hydrogen+production+through+steam+electrolysis%3A+Model-based+dynamic%0D%0Abehaviour+of+a+cathode-supported+intermediate+temperature%0D%0Asolid+oxide+electrolysis+cell&sca_esv=602061605&sxsrf=ACQVn08p8SHl4qM2hGHtIkW6aSru7Iw%3A1706399633709&ei=kZe1ZbvtKrLji-gPruqm0AQ&ved=0ahUKEwj7-YuA4v6DAxWy8QIHHS61CUoQ4dUDCuact=5&oq=Hydrogen+production+through+steam+electrolysis%3A+Model-based+dynamic%0D%0Abehaviour+of+a+cathode-supported+intermediate+temperature%0D%0Asolid+oxide+electrolysis+cell&gs_lp=Egxnd3Mtd2l6LXNlcnAimwFIeWRyb2dlbiBwcm9kdWN0aW9uIHRocm91Z2ggc3Rlc sclient=gws-wiz-serp (visited on 01/27/2024).

[20] Søren Højgaard Jensen. "Solid Oxide Electrolyser Cell." In: ().

[21] Daniel G. Milobar, Joseph J. Hartvigsen, and S. Elangovan. "A techno-economic model of a solid oxide electrolysis system." In: *Faraday Discussions* 182.0 (Nov. 3, 2015). Publisher: The Royal Society of Chemistry, pp. 329–339. URL: https://pubs.rsc.org/en/content/articlelanding/2015/fd/c5fd00015g (visited on 01/27/2024).

[22] Ardemis Boghossian. *Electrochemical Engineering*. EPFL Lecture. Fall 2023.

[23] *An overview of water electrolysis technologies for green hydrogen production - ScienceDirect*. URL: https://www.sciencedirect.com/science/article/pii/S2352484722020625 (visited on 12/28/2023).

[24] Dr Fabio Oldenburg. *Key electrolyzer technologies and their roles in the future green hydrogen project landscape*. Apricum - The Cleantech Advisory. Oct. 17, 2022. URL: https://apricum-group.com/which-horse-to-bet-on-key-electrolyzer-technologies-and-their-roles-i (visited on 12/28/2023).

[25] Prashik S. Gaikwad et al. "Enhancing the Faradaic efficiency of solid oxide electrolysis cells: progress and perspective." In: *npj Computational Materials* 9.1 (Aug. 21, 2023). Number: 1

Publisher: Nature Publishing Group, pp. 1–14. URL: https://www.nature.com/articles/s41524-023-01044-1 (visited on 02/08/2024).

[26] Luca Mastropasqua and Jack Brouwer. "Solid Oxide Electrolysis Cells (SOEC) integrated with Direct Reduced Iron (DRI) plants for producing green steel." In: ().

[27] Kyle Buchheit et al. *Solid Oxide Cell and Stack Manufacturing Cost Tool*. DOE/NETL-2022/3230, 1842506. Jan. 14, 2022, DOE/NETL–2022/3230, 1842506. URL: https://www.osti.gov/servlets/purl/1842506/ (visited on 12/28/2023).

[28] *The Pros and Cons of Hydrogen Energy Storage*. CLOU GLOBAL. June 18, 2023. URL: https://clouglobal.com/the-pros-and-cons-of-hydrogen-energy-storage-is-worth-the-invest (visited on 12/28/2023).

[29] Meiting Guo et al. "Optimization Design of Rib Width and Performance Analysis of Solid Oxide Electrolysis Cell." In: *Energies* 13 (Oct. 19, 2020), p. 5468.

[30] Zheng Cao, Shengli An, and Xiwen Song. "Effect of thermal treatment at high temperature on phase stability and transformation of Yb2O3 and Y2O3 co-doped ZrO2 ceramics." In: *Scientific Reports* 12.1 (June 15, 2022). Number: 1 Publisher: Nature Publishing Group, p. 9955. URL: https://www.nature.com/articles/s41598-022-13705-0 (visited on 12/29/2023).

[31] E. Ivers-Tifféea A. Leonidea Y. Apela. "SOFC Modeling and Parameter Identification by Means of Impedance Spectroscopy." In: *The Electrochemical Society* (2009), p. 30. URL: https://iopscience.iop.org/article/10.1149/1.3247567.

[32] Shengyue Lu. "Economies of Scale in PEMEC and SOEC Manufacturing based on a Bottom-up Model." In: *I nfoscience EPFL* 13 (2022), p. 5468. URL: https://infoscience.epfl.ch/record/296756?ln=fr.

[33] Roberto Scataglini et al. "A Total Cost of Ownership Model for Solid Oxide Fuel Cells in Combined Heat and Power and Power-Only Applications." In: ().

[34] Mark R. Weimar et al. *Cost Study for Manufacturing of Solid Oxide Fuel Cell Power Systems*. PNNL–22732, 1126362. Sept. 30, 2013, PNNL–22732, 1126362. URL: http://www.osti.gov/servlets/purl/1126362/ (visited on 12/29/2023).

[35] Saddam Hussain and Li Yangping. "Review of solid oxide fuel cell materials: cathode, anode, and electrolyte." In: *Energy Transitions* 4.2 (Dec. 1, 2020), pp. 113–126. URL: https://doi.org/10.1007/s41825-020-00029-8 (visited on 01/25/2024).

[36] David A. Tucker et al. *Fuel utilization effects on system efficiency and solid oxide fuel cell performance in gas turbine hybrid systems*. NETL-PUB-20799. National Energy Technology Laboratory (NETL), Pittsburgh, PA, Morgantown, WV (United States), Sept. 13, 2016. URL: https://www.osti.gov/biblio/1618273 (visited on 01/26/2024).

[37] *Frontiers | A Cogeneration System Based on Solid Oxide and Proton Exchange Membrane Fuel Cells With Hybrid Storage for Off-Grid Applications*. URL: https://www.frontiersin.org/articles/10.3389/fenrg.2018.00139/full (visited on 01/26/2024).

[38] *DOE Hydrogen and Fuel Cells Program Record - Energy Requirements for Hydrogen Gas Compression*. https://www.hydrogen.energy.gov/docs/hydrogenprogramlibraries/pdfs/19001_hydrogen_liquefaction_costs.pdf.

[39] Amgad Elgowainy et al. "Techno-economic and thermodynamic analysis of pre-cooling systems at gaseous hydrogen refueling stations." In: *International Journal of Hydrogen Energy* 42.49 (Oct. 16, 2017). Institution: Argonne National Lab. (ANL), Argonne, IL (United States) Publisher: Elsevier. URL: https://www.osti.gov/biblio/1422579 (visited on 01/26/2024).

[40] Jamie Holladay and Pacific Northwest National Laboratory. "Magnetocaloric Hydrogen Liquefaction." In: (2019).

[41] *Gaseous Hydrogen Compression*. Energy.gov. URL: https://www.energy.gov/eere/fuelcells/

gaseous-hydrogen-compression (visited on 01/26/2024).

[42] Cassidy Houchins and Brian D. James. *Hydrogen Storage Cost Analysis*. Presentation at DOE Hydrogen Program 2022 Annual Merit Review and Peer Evaluation Meeting. Project ID: ST235. DOE Hydrogen Program, June 2022. URL: https://www.hydrogen.energy.gov/pdfs/review22/st235_houchins_2022_p.pdf.

[43] *Hydrogen Storage*. Pure Energy Centre. URL: https://pureenergycentre.com/hydrogen-products-pur hydrogen-storage/ (visited on 01/27/2024).

[44] *Compressed hydrogen storage*. MAHYTEC. URL: https://www.mahytec.com/en/compressed-hydrogen- (visited on 01/27/2024).

[45] Andreas Züttel. *Hydrogen Storage*. Lecture Slides. Lecture given on 13 October 2023. École Polytechnique Fédérale de Lausanne (EPFL), 2023.

[46] *Groupe E produces first green hydrogen molecules at Swiss site*. Renewablesnow.com. URL: https://renewablesnow.com/news/groupe-e-produces-first-green-hydrogen-molecules-at-swis (visited on 01/27/2024).

A Heat Model

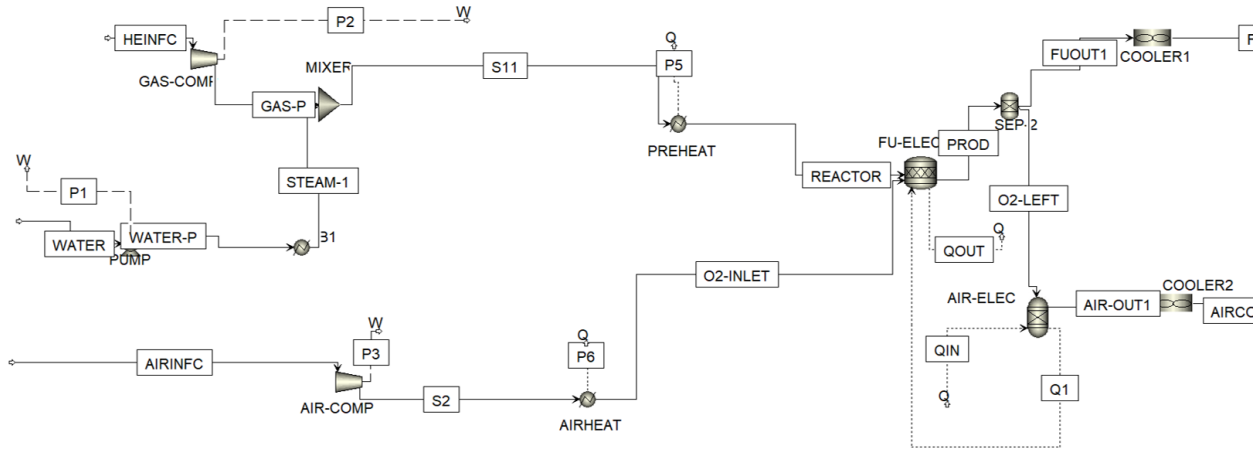

Figure 26: Current status overview of the heat model in Aspen